

MOEMS based on Magnetic/Photonic Sensitive Stimuli Polymers

Sandra de Pedro i Jordán

Doctorat en Física

Bellaterra 2014

Universitat Autònoma de Barcelona

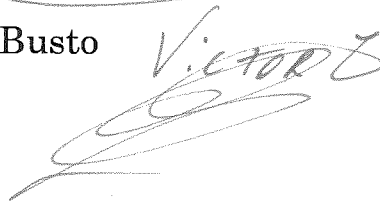
Departament de Física Òptica

Directors:

Dr. Andreu Llobera Adán



Dr. Víctor Javier Cadarso Busto



Tutor:



Dr. Jordi Mompert Pepina



Index

O verview and motivation	5
References	6
1. I ntroduction	7
Magnetic sensitive polymers	14
Light sensitive polymers	16
Objectives addressed in this Thesis	20
Magnetic actuated polymers	20
Light actuated polymers	21
References	24
2. R esults & Discussion	31
2.1. Magnetic-sensitive stimuli material	31
2.1.1. Magnetic-sensitive stimuli material synthesis	31
2.1.2. Magnetic-sensitive stimuli material characterization	32
Polymerization	32
Nanoparticles distribution	32
Magnetization	34
Biocompatibility	36
Mechanical properties	38
Optical properties	40
2.1.3. Magnetic-sensitive stimuli material implementation in MOEMS	43
Mechanical characterization	47

Index

Optical characterization	49
2.2. Light-sensitive stimuli material	52
2.2.1. Light-sensitive stimuli material synthesis	53
2.2.2. Light-sensitive stimuli material Epocore based: photopatternable study test structures	53
Photopatternable study	53
2.2.3. Light-sensitive stimuli material Epocore and SU-8 test structures	54
Design	54
Fabrication	55
Optical characterization	56
Red light-sensitive stimuli SU-8 based	58
Optical characterization	59
Thermal Properties	60
2.2.4. Red light sensitive stimuli SU-8 based implemented on a VOA- MOEMSs	60
Design	60
Optical simulations	61
Fabrication	62
Optical characterization of red light-sensitive stimuli implemented into VOA-MOEMS	64
References	67
3. Compendium of articles	71
4. Conclusions	131
5. Appendixes	135

Overview and motivation

This thesis, structured by article compendium, summarizes the research work performed at the *Centro Nacional de Microelectrónica* (IMB-CNM, CSIC) by the author from 2009 to 2014 in order to obtain the PhD degree in Physics at the *Universitat Autònoma de Barcelona*. It can be considered as the logical continuation from previous Ph.D. done at IMB-CNM (CSIC) by Dr. C. Martin-Olmos [1] and Dr. V.J. Cadarso-Busto [2] and the main topic is to further develop polymer-based micro-opto-electromechanical systems (MOEMS) concept able to be actuated by two different physical external stimuli: magnetism and light.

In her Ph.D. Thesis, Dr. C. Martin-Olmos, developed polymer-based functional materials (using Poly(Methyl Methacrylate) (PMMA) and SU-8 as base polymer) for micro- and nano- systems (MEMS and NEMS, respectively). In the frame of that thesis, two epoxy-based materials with added functional properties arising from γ -Fe₂O₃ nanospheres or TiO₂ nanorods were developed. Such materials were mechanically characterized by using an indentation test. Non-doped epoxy samples had a Young's modulus (Y) of 4.6 GPa. With the inclusion of the nanoparticles, Y increased until 7.54 GPa and 7.62 GPa for γ -Fe₂O₃ and TiO₂, respectively. Additionally, when using iron oxide nanoparticles (in a concentration of $6 \cdot 10^{-6}$ mol/g), it was obtained a magnetic sensitive stimuli material (M-SSM) [3] which was used for the fabrication of atomic force microscopy (AFM) probes. These probes comprised a cantilever ended in a sharp tip [4].

The resonant frequency (ω) and the quality factor (Q) for cantilevers obtained with the γ -Fe₂O₃-based M-SSM were experimentally studied in two operational modes working in either air or liquid media. For the first case, ω values ranging from 271 kHz to 4 kHz (corresponding to 100 μ m and 800 μ m AFM probe lengths, respectively) and

Overview and motivation

Q values ranging from 289 to 27 (corresponding to 100 μm and 800 μm AFM probe lengths, respectively) were obtained. Q increased as compared to the epoxy based resist cantilevers and decreased as a function of the cantilever length. Under liquid operation mode, ω values of 7 kHz and 9 kHz (for 500 μm and 400 μm AFM probe lengths) and Q values of 34 and 40 were experimentally obtained (for 500 μm and 400 μm AFM probe lengths, respectively).

In the second part of the work presented by Dr. C. Martin-Olmos, a polymer doped with polyaniline emeraldine (PANI-EB) base was used to implement an optothermal cantilever. Actuation was achieved by focusing a laser beam on a specific region of the microsystem, where light was absorbed by the PANI-EB, increasing the temperature of the material (due to Joule effect) resulting on a cantilever displacement. This displacement was studied as a function of the relative position of the laser spotted along the cantilever length. From the experimental results, a maximum deflection close to 70 μm was achieved.

The Ph.D. work from Dr. V. J. Cadarso-Busto, was focused on the development and/or improvement of non-conventional technologies for microfabrication: i) Deep Reactive Ion Etching (DRIE) process was optimized to develop MOEMS and micro-optical structures, as could be silicon-based rectangular hollow waveguides [5]. Such structures showed total losses close to 6.0 dB for a length of 3.0 cm. ii) Use of photopatternable polymers for Micro-Opto-electromechanical Systems (MOEMS) and micro-optics. Here, the polymer was used for obtaining both optical accelerometers [6] and variable optical attenuators [7]). In both cases, the MOEMS consisted on a seismic mass anchored to a frame by four mechanical beams (quad beam approach) [8]. This configuration assured that the displacement of this mass was flat (i.e. without tilting). Measurement was done by placing a waveguide at the seismic mass (thus able to move with the seismic mass) and two waveguides located at the frame. When related to variable optical attenuators (VOAs) [9], an additional Aluminium layer was deposited over the optical accelerometers. When a voltage was applied the mechanical beams were heated and expanded, with the final result of achieving an overall displacement of the seismic mass and, straightforwardly, a misalignment between the waveguide located at the mass and those at the frame. Thus,

Overview and motivation

in both cases, the light intensity coupled to the waveguides was modulated either by the acceleration or by the applied voltage.

Grounded on these aspects, SU-8 accelerometers were optimized, specially the junction between the mechanical beams and the inertial mass so as to minimize mechanical stresses. Moreover, optical sensitivities were studied obtaining values ranging between 11.12 dB/g and 32.14 dB/g (depending on the specific geometries). When measuring VOAs, optical losses of 20 dB with only 12 mW of power consumption were achieved. iii) Finally, soft lithography was used for the development of Polydimethylsiloxane (PDMS) cantilevers [10]. With regard to the case of PDMS cantilevers, resonant frequencies were studied both numerically and experimentally, having identical values (83 ± 1 Hz) for a cantilever length of 2400 μm . Such system presented relative losses of 25 dB when an ethanol droplet (2 μl or equivalently 1.58 mg) was dispensed on the cantilever.

Thus, the thesis here presented is inspired on the functionalized materials as well as the actuation principles and materials with tuneable optical properties presented in the work of Dr. C. Martin-Olmos (magnetic and opto-thermal materials) and on the fabrication techniques and systems developed by Dr. V.J. Cadarso-Busto (soft- and , photolithography, MOEMS). Accordingly, this thesis is focused on the development of MOEMS based on new polymeric functionalized materials. Concretely, PDMS cantilevers acting as VOA are achieved by obtaining M-SSMs based on PDMS and ferrofluid (FF). Additionally, light-sensitive materials based on SU-8 and color dyes are characterized and implemented in an all-polymer light actuated VOAs. Each of these systems is obtained with the most suitable technology, such as soft lithography, ink jet printing or UV-lithography and detailed information is presented throughout this work.

This work is divided in 4 different chapters aiming to provide a general view of the work done, as well as a discussion of the obtained results:

Chapter 1, *Introduction*, presents a review of the state of the art of fabrication techniques and actuable materials used on the development of MEMS and MOEMS. Moreover, the functionalized material concept is introduced, focusing on the magnetic and light sensitive stimuli materials.

Overview and motivation

Chapter 2, *Results and discussion*, is divided in two sections: the first one corresponds to the magnetic actuated elastomer and the second one to the light actuated polymer. The study of those materials, their implementation in the fabricated systems and the results obtained are here discussed. In the first case the M-SSM is obtained by mixing the polymer and the FF. Afterwards, this M-SSM is characterized (structural, optical, magnetic, mechanical and biocompatibility) and further implemented in a VOA. For the second case, the material is obtained and optically characterized. Once optimized, it is used to define a VOA-MOEMS.

Chapter 3, *Compendium of articles*, presents the articles that form this thesis. There are two articles which have been published during the elaboration of this thesis and there are two more that are in the process of correction which are also included. The published articles are:

1. S.de Pedro, A. Voigt, V. J. Cadarso, J. Vila-Planas, J. Brugger, S. Büttgenbach, A. Llobera, G. Gruetzner, "UV-patternable polymers with selective spectral response", *Microelectronic Engineering*, vol. 98, pp. 234-237, Oct. 2012, IF: 1.295(2011), Subject area: Material Science: Electronic, Optical and Magnetic Materials, Rank: 0.572.
2. S.de Pedro, V. J. Cadarso, X. Muñoz-Berbel, J. A. Plaza, J. Sort, J. Brugger, A. Llobera, "PDMS-based, magnetically actuated variable optical attenuators obtained by soft lithography and inkjet printing technologies", *Sensors and Actuators A: Physical*, vol. 215, pp. 30-35, Jan. 2014, IF: 2.116 (2014), Subject Area: Material Science: Electronic, Optical and Magnetic Material, Rank: 0.883.7

The next article has been sent to "Journal of Micromechanics and Microengineering". Reviewers from this magazine have been sent to me their comments / corrections for its subsequent publication. It should be said, that today's date it has been accepted and published:

3. S de Pedro, V. J. Cadarso, T. Ackerman, X. Muñoz-Berbel, J. A. Plaza, J. Brugger, S. Büttgenbach, A. Llobera, "Polymeric variable optical attenuators based on magnetic sensitive stimuli materials", *Journal of Micromechanics and Microengineering*, vol. 24, pp. 14, Sept. 2014, IF: 1.597 (2014), Subject

Overview and motivation

area: Material Science: Electronic, Optical and Magnetic Material, Rank: 0.726.

4. S de Pedro, X. Muñoz-Berbel, R. Rodríguez-Rodríguez, J. Sort, J. A. Plaza, E. Mendoza, J. Brugger, A. Llobera and V. J. Cadarso, “Preparation and Characterization of Patternable Magnetic Stimulus Sensitive Elastomers Obtained from Mixtures of PDMS and Ferrofluid”.
5. S de Pedro, T. Ackermann., J. A. Plaza., L. Thomas, E. Alvarez, A. Vierheller, S. Büttgenbach, V. J. Cadarso and A. Llobera, “All-photoinc SU-8 variable optical attenuator”.

Chapter 4, *Conclusions*, presents a summary of the main obtained results on this thesis.

REFERENCES

- [1] C. Martín Olmos, “Micro/Nano fabrication of polymer-based devices,” Universitat Autònoma de Barcelona, 2008.
- [2] V. J. Cadarso, “Non conventional technologies for integrated optics,” Universitat Autònoma de Barcelona (UAB), 2008.
- [3] C. Ingrosso, C. Martin-Olmos, A. Llobera, C. Innocenti, C. Sangregorio, M. Striccoli, A. Agostiano, A. Voigt, G. Gruetzner, J. Brugger, F. Perez-Murano, and M. L. Curri, “Oxide nanocrystal based nanocomposites for fabricating photoplastic AFM probes,” *Nanoscale*, vol. 3, no. 11, pp. 4632–9, Nov. 2011.
- [4] C. Martin, A. Llobera, G. Villanueva, A. Voigt, G. Gruetzner, J. Brugger, and F. Perez-Murano, “Stress and aging minimization in photoplastic AFM probes,” *Microelectron. Eng.*, vol. 86, no. 4–6, pp. 1226–1229, Apr. 2009.
- [5] V. J. Cadarso, A. Llobera, I. Salinas, D. Izquierdo, I. Garcés, and C. Domínguez, “Silicon-based rectangular hollow integrated waveguides,” *Opt. Commun.*, vol. 281, no. 6, pp. 1568–1575, Mar. 2008.
- [6] A. Llobera, V. Seidemann, J. A. Plaza, V. J. Cadarso, and S. Buttgenbach, “SU-8 Optical Accelerometers,” *J. Microelectromechanical Syst.*, vol. 16, no. 1, pp. 111–121, Feb. 2007.
- [7] A. Llobera, G. Villanueva, V. J. Cadarso, V. Seidemann, S. Buttgenbach, and J. A. Plaza, “Polymer Microoptoelectromechanical Systems: Variable Optical Attenuators and Accelerometers,” in *TRANSDUCERS 2007 - 2007 International Solid-State Sensors, Actuators and Microsystems Conference*, 2007, pp. 1079–1082.
- [8] J. A. Plaza, A. Llobera, C. Dominguez, J. Esteve, I. Salinas, J. Garcia, and J. Berganzo, “BESOI-Based Integrated Optical Silicon Accelerometer,” *J. Microelectromechanical Syst.*, vol. 13, no. 2, pp. 355–364, Apr. 2004.
- [9] A. Llobera, G. Villanueva, V. J. Cadarso, S. Battgenbach, and J. A. Plaza, “Polymeric MOEMS Variable Optical Attenuator,” *IEEE Photonics Technol. Lett.*, vol. 18, no. 22, pp. 2425–2427, Nov. 2006.
- [10] A. Llobera, V. J. Cadarso, K. Zinoviev, C. Dominguez, S. Buttgenbach, J. Vila, J. A. Plaza, and S. Biittgenbach, “Poly(Dimethylsiloxane) Waveguide Cantilevers for Optomechanical Sensing,” *IEEE Photonics Technol. Lett.*, vol. 21, no. 2, pp. 79–81, Jan. 2009.

1. Introduction

The first micro-electro-mechanical system (MEMS) was presented at the end of 1970s, as a direct result derived from the development of silicon micromachining technologies for creating miniaturized sensors and actuators [1]. Such MEMS did not become a large scale product until in the 90's [2], when these technologies were mature enough to provide with yields high enough from a mass production point of view. This was actually triggered by the parallel development of two silicon-based technologies for MEMS: bulk and surface micromachining [3]. As the name indicates, the first one allows defining 3D features by etching (chemically or physically) the material in bulk, whereas surface micromachining is related to the technologies where the features are building up, layer by layer, on the substrate surface. As a result, hitherto it is possible to find in the literature a myriad of different MEMS suitable to measure either physical, chemical or biochemical magnitudes, such as displacement [4], pH [5] or velocity [6]. Focused on the measurement of physical magnitudes, the acceleration has been of key importance during the last few decades, mainly because of its huge field of application, which ranges from automotive (airbags) through health (posture recognition) to aerospace (satellite positioning). Due to this massive effort, MEMS-based accelerometers with small size and weight, low-power consumption and low price can be found in both the market and in the literature [7]. Despite these interesting properties, accelerometers, and MEMS in general still present some drawbacks that limit their performance: i) temperature dependence, preventing their applicability in regions with large temperature variations (i.e. outer space); ii) high-cross sensitivity to electromagnetic interferences (EMIs) limiting its use under strong applied magnetic fields; iii) necessity of complex *in situ* data readout system (including pre-amplifiers). The latter issue hampers its use at harsh/explosive environments due to the possibility of a shortcut leading to spikes.

1. Introduction

A potential solution to these limitations is the replacement of electrons by photons as transduction mechanism, that is, the combination of micro-optics or integrated optics and MEMS obtaining what has been known as micro-opto-electromechanical system (MOEMS). Several unique light properties (such as changes in intensity [8], wavelength [9] or phase [10]) can be used to obtain micromechanical systems with the following characteristics: i) high sensitivity and thermal stability; ii) immunity to EMIs, hence applicable under strong electromagnetic fields and iii) easy readout system, which may only require a photodetector and a cheap light source (as could be a light emitting diode, LED). Moreover, these MOEMS can be positioned far away from the measured zone (by using fiber optics for interconnection) allowing its use in harsh environments. Grounded on these advantages, it is not surprising why the MOEMS concept has evolved from sensing a given magnitude (analogous to the MEMS) to being able to be actuated when a specific stimulus is applied. Some of these actuated MOEMS have overpassed the research level and can be found in a technical readiness level 9 (TRL9), meaning being in the market. In this context, actuable MOEMS already have a place in our everyday life, as they can commercially be found in applications such as imaging, microscopy, endomicroscopy, robotic surgery and cell-phone cameras [11], [12]. An example of such MOEMS is the variable focus lenses presented by S. J. Lukes [11]. It consists on a commercial confocal microscope based on the controlling of a MEMS focusing mirror inserted into the beam path of the confocal microscope. This system is used for acquiring high-resolution image data along biologically or clinically relevant cross-sections. A second example are the iris micro-shutters, where a microfluidic iris with tunable range from 4.2 to 0.85 mm in diameter and tuning ratio of 80 % is reported by J. H. Chang [13]. The turnaround speed is 80 mm/s which is higher than other adaptive liquid iris [14] [15]. Brant M. Kaylor, *et al* [16], presented a miniaturized non-mechanical zoom camera using deformable MOEMS mirrors. In that case, the Bridger Photonics, Inc. (Bridger) in collaboration with Montana State University (MSU) developed electrostatically actuated deformable MEMS mirrors for use in compact focus control and zoom imaging systems [16].

In addition, there is an even bigger field of applications still at research level, such as moduable micro-optics [17]. Specifically, some examples are: i) a MOEMS filter is shown in the work leaded by O. Haitham [18], with a wavelength rejection ratio better than 20 dB. The reported filter is suitable for the production of integrated swept

1. Introduction

sources (fast wavelength scanning light source) for optical coherence tomography. ii) A MOEMS scanner composed of a device section with comb electrodes and a tilting section [19]. The fabricated microscanner shows an optical scan angle of up to 4.23° at 90 V in the static mode and stable actuation of up to 11.3° at resonant frequency (ω) of 2.87 kHz. The initial tilted angles in the microassembly process show high repeatability within 10 % error. iii) B. Reig, *et al* [20], demonstrated a low-cost fabrication technique of a polymer MOEMS suited for dynamic focusing of vertical-cavity surface emitting lasers (VCSELS). These MOEMS allows a vertical displacement of around $0.2 \mu\text{m/W}$ with a maximal range of $8 \mu\text{m}$. iv) Z. Kazem, *et al*, [21] developed MOEMS accelerometers which are designed for micro-satellite navigation. The sensor response to the acceleration ranging from 0 to 0.7 g is approximately linear; with a sensitivity of 1.6 dB/g. v) MOEMS-based wavelength-selective switches (WSSs) able to demultiplex, switch and re-multiplex can be found in the work by J. Canning [22], where two consecutive long-period-gratings separated by 100 nm interfere with high visibility allowing to switch easily between the core and the cladding mode. This can be done with a small wavelength shift of 3.2 nm, corresponding to a signal switching contrast better than 14 dB.

Moreover, it is also important to mention seminal examples which are expected to play a key role not only in telecommunications applications, but also in other apparently distant fields such as biology analytical chemistry. Only to provide some examples, modifiable micro-optics with magnetic actuation is developed by N. Weber *et al*, [23], (Figure 1.1(a)). Concretely, angular deflections of a micromirror are achieved by magnetically-actuating (using integrated or ultra-miniaturized coils) a patterned magnetic polymer. In that case deflection angles of up to 9° for magnetic fields of a few microteslas ($6 \mu\text{T}$) when working in resonance, which are increased to militeslas ($2 \text{ mT} - 8 \text{ mT}$) for static deflection are obtained. Moreover, the original maximum amplitude is restored by varying the operating frequency by only 100 mHz. In such systems no electrical wiring is required for the mirrors, enabling its assembly in platforms and thus used in imaging endoscopy, as for example in optical endoscopic diagnostics. Secondly, a dynamically reconfigurable liquid lenses in a microfluidic channel are demonstrated by S. K. Y. Tang, *et al* [24]. In Figure 1.1(b) a schematic diagram of the device and how it focuses light from an optical fiber through the liquid lens is shown. Specifically, in such configuration the laminar flow of three streams of liquids in a microchannel form a

1. Introduction

liquid-core liquid-cladding (L2) lens. By manipulating the relative flow rates of the streams its shape is reconfigured, thus varying the lens focal distance. Different shapes of the lens are obtained as a function of the rate flow (biconvex, plano-convex or convex). The focal distance range is from 5 mm to 12 mm for the flows rate of 2 ml/h to 9 ml/h.

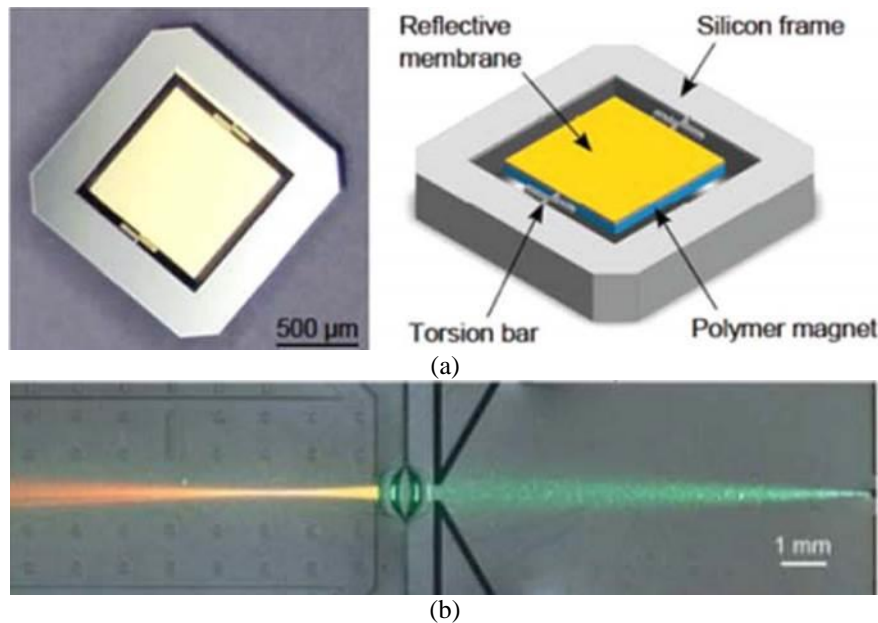


Figure 1.1: (a) Photograph of (left) the magnetic micromirror. The polymeric magnet is attached to the back side of the mirror membrane, as shown in (right) the 3-D model [23]. (b) Bright-field image of the lens with a green laser beam from the fiber in front of the lens. The focused beam in the beam-tracing chamber is orange due to the fluorescence of the dye[24].

Among the different MOEMS already discussed, probably variable optical attenuator (VOA) has become a key component in telecommunications applications, specifications such as low insertion loss ($IL < 1$ dB) [25], large attenuation range ($AR > 30$ dB) [26], high response speed ($RS < 1$ ms), spectral bandwidth ($SB > 100$ nm) and small polarization dependence loss ($PDL < 0.5$ dB) are demanded [27], [28]. Currently, the most common VOAs are opto-mechanical, which provide large $AR > 50$ dB and fine resolution (0.1 dB), but their $RS > 0.5$ s, bulky size and high cost hampers their applicability. MOEMS approach has as major advantages the small size (< 1 cm²), the batch fabrication and the low cost [25], [29]–[31]. Thus, VOAs are one of the most promising configurations for light intensity control on a photonic circuit, and as such, there has been a considerable effort towards its development. Examples can be found in the literature with outstanding performance, such as these based on a vertical comb drive shown in Figure 1.2(a). Here, an actuated silicon micromirror combined with an

1. Introduction

optical fiber collimator is presented. The VOA operates at a driving voltage of 4.4 V with a turn-on and turn-off response time of 1.6 ms and 2.74 ms, respectively and optical attenuation of 40 dB [32]. An additional VOA based on a mechanical anti-reflection switch for modulation applications is shown in Figure 1.2(b). In this case, a linear response of attenuation vs voltage is shown, with the additional feature of providing an attenuation up to 5.6 dB when applied voltage was changed from 0 to 15 V [33]. Important is here to mention that, albeit presenting outstanding performance, most of the state of the art VOAs are based on silicon-derived technology making them fragile. In addition, in some of them, highly-precise technological steps are required, dramatically increasing its cost (and/or reducing its yield), which limits their mass implementation.

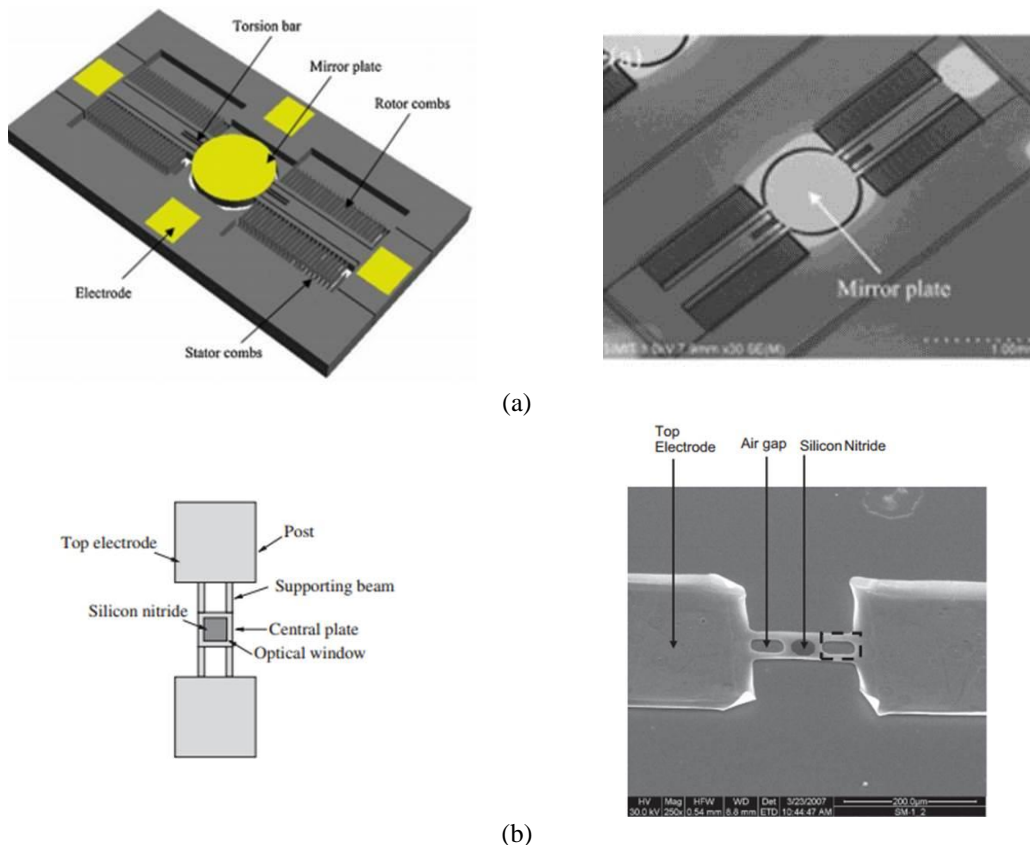


Figure 1.2: (a) Schematic diagram of a micromirror (left) and a SEM image of fabricated micromirror with vertical comb drive (right) [34]. (b) Top view of the VOA system (left). SEM picture of a released system, showing the full system (right) [33].

To tackle this fragility, a second family of VOAs have been developed, which are based on planar lightwave circuits (PLC) [35]. They are nowadays preferred in

1. Introduction

robust wavelength division multiplexing (WDM) applications since they do not have movable parts (and therefore having higher mechanical robustness). In addition, they can be integrated (either monolithically or with heterogeneous integration) with other systems such as optical switches or wavelength multiplexers [36], [37]. Despite these improvements, VOAs based on PLC still present constraints, being the most important the voltages in the order of tenths of volt.

In addition to the previously mentioned WDM applications, there exist other situations where optical power control is required, such as to avoid photodamage of optical membranes in chemical sensors [38] or to control phototoxicity in cell cultures [39]. In this context, VOAs are progressively being used. Therein, key aspects in WDM such as response speed (RS) and polarization dependence loss (PDL) become less important as compared to mechanical robustness, large spectral bandwidth ($SB > 500$ nm) and biocompatibility. To address the associated challenges of this second kind of applications, polymer technology is predominantly used [40]. In general, polymers [41] present attractive properties like: i) lower Young's modulus (Y) (e.g. PDMS, PMMA or polystyrene, PS; $Y_{PDMS}=800$ KPa, $Y_{PMMA}=2.4$ MPa, $Y_{PS}=3.5$ GPa, respectively) than silicon ($Y_{Si}=169$ GPa). Here, a decrease in the Y brings a relaxation of the MOEMS design and fabrication constraints (specially their dimensions). This has allowed to define larger MOEMS with similar mechanical properties and sensitivities than their silicon-based counterparts, but using a more robust technology; ii) polymers can be considered as low cost materials, even with the possibility to be processed outside the clean room; iii) outstanding optical properties, with high transmittance in a broad wavelength range (from UV to IR), as opposite to silicon, which is only transparent for wavelengths above 1100 nm; iv) possibility to be functionalized either in surface or in bulk, conferring the final material with additional properties which arise from the specific dopants used (change in spectral response, sensitive to electromagnetic fields, etc.).

Functionalization has been one of the hot topics in material science and surface chemistry for decades [42], [43]. To date, materials whose properties (optical, mechanical chemical, etc.) can be modulated as a function of an external stimulus (like changes in pH [44], temperature [45], electric fields [46] and/or magnetic fields [47]) are broadly known as sensitive stimuli materials (SSMs) [48]. Generally, any SSM consists on a non-actuable host matrix and a filler (also called dopant or additive) with

1. Introduction

compatible physicochemical properties. Among the different SSMs, these suitable to change their shape under non-contact stimulus such as magnetism [49] or optics [50] are preferred for in vivo applications because of their contactless actuation and operation simplicity [51]. There is a variety of matrices which are used in the development of SSMs including metals, ceramics and polymers [52]. Specially these latter are taking a pre-eminent position since they can be functionalized in bulk (as opposite to ceramic, semiconductor or metals, where only surface functionalization can be done). In addition, the matrix assures the physical (and sometimes chemical) entrapment of the filler inside the polymer. Thus, if the matrix is mechanically and chemically stable, no dopant (or sub-products) leach occurs, which is especially important in biological/biomedical applications. Elastomers are a kind of polymers which have become of interest for defining a specific type of SSM. Among the different elastomers available, PDMS has mostly been used as host matrix material, since it has outstanding properties such as: i) low Y , as above discussed [53], being then suitable for elastic (non-plastic) structures; ii) high transmittance in the UV-NIR range ($> 80\%$) [54] (which allows implementing the so-called photonic lab on a chip [55]); iii) biocompatibility [56] i.e. it is used in the development of implantable drug delivery systems [57]; iv) long thermo-chemical and structural stability [58]; v) fabrication simplicity [59] and vi) low cost [60].

The filler properties are also crucial, since they have to be selected in accordance to the actuation principle to be used. Among the different examples that can be found in the literature, it is worth highlighting the work presented by R. S. Scott, *et al* [61], who have implemented a pH responsive hydrogel that undergo shape changes in response to specific wavelengths of light stimuli as controllable valves in microfluidics (Figure 1.3). Furthermore, the work presented by Ziriny and co-workers, who synthesized a lightly crosslinked PDMS containing charged components (TiO_2 particles) [62]. This is clearly represented in Figure 1.4 where the bending of the gel in combination with the particles of TiO_2 as a response to an electromagnetic field stimulus is observed.

1. Introduction

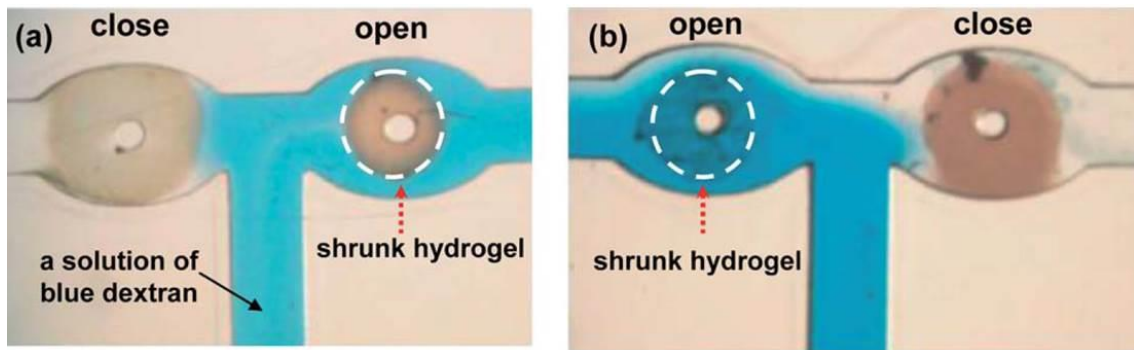


Figure 1.3: Two valves at a T-junction in a microfluidic system are made of different nanocomposite hydrogels doped with gold colloid (right) and gold nanoshell (left), respectively. A) When exposed to green light, the gold colloid valve opened while the nanoshell valve remains close; b) when the system is exposed to near infrared light, the opposite response is observed [61].

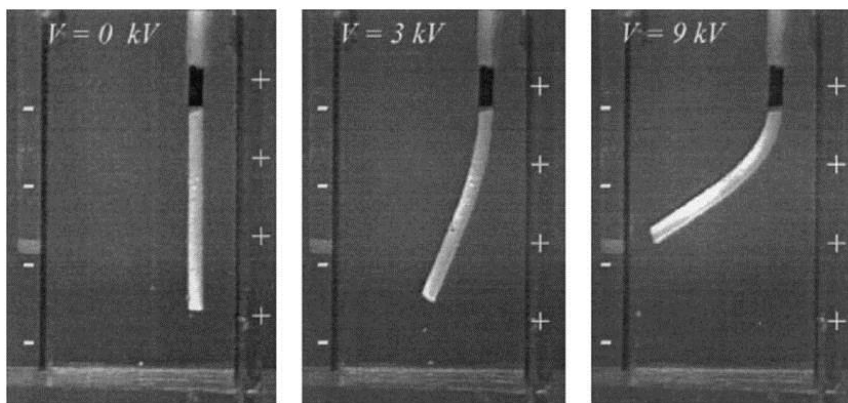


Figure 1.4: Electro-response of a PDMS gel loaded with 10% TiO₂ as a function of uniform field strength [62].

Magnetic sensitive polymers

The implementation of magnetically-actuable SSM (M-SSM) has been widely reported in the literature, considering that it is a simple actuation mechanism that may provide with actuation forces in the order of hundreds of mN [63]. It has been demonstrated that a M-SSM can be obtained using magnetic nanoparticles (MNPs) as additive in PDMS matrices [64], [65]. These materials have shown large shape tunability and mechanical behaviour as a function of the dispersion, distribution, morphology and loading of the MNPs [66]. F. N. Pirmoradi *et al.*, [67] has reported a drug delivery system which is magnetic actuated for controlling drug release. It consists on a M-SSM membrane (6 mm x 40 μ m of diameter) which has been made of PDMS and iron oxide nanoparticles (Fe₃O₄) coated with an acid surfactant. The magnetic nanoparticles have been dispersed into the PDMS matrix in weight content close to 70%. With an applied magnetic field of 2 G, a maximum deflection of 350 μ m is achieved. In Figure 1.5, the fabricated prototype of the drug delivery device is presented. Dimensions of such system are 6 mm in diameter and 550 μ m in depth for

1. Introduction

the drug-loaded micro reservoirs and 6 mm in diameter and 40 μm thicknesses for the magnetic membranes. Moreover, the membrane presents a 210 μm diameter aperture. Here, intermittent magnetic actuation of the device (2 kG magnetic field) causes a release of the methylene blue (MB) through the 210 μm diameter aperture. An example of the combination of PDMS and iron oxide nanoparticles dispersed in a liquid carrier for implantable systems can be found at [68], where a 7 mm-diameter, 35 μm -thick loaded with 40 wt % is reported. In Figure 1.6 the deflection of this magnetic membrane is observed as the magnetic field source is located close to the magnetic material, achieving a deflection of 625 μm for an applied magnetic field of 4.1 kG. Such magnetic PDMS membranes may be used in micro-pumps and lab-on-a-chip applications.

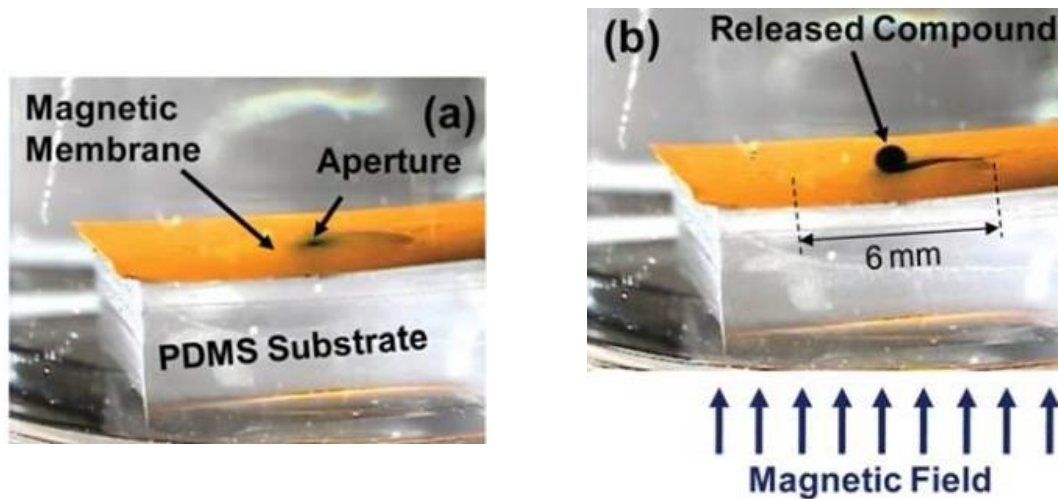


Figure 1.5: A prototype system in water, fabricated with 6 mm diameter membrane and 210 μm aperture diameter, (a) no magnetic field is present. (b) After the application of a magnetic field of 2G for underneath the system. Magnetic actuation results in discharge of methyl blue (MB) from the system [67].

1. Introduction

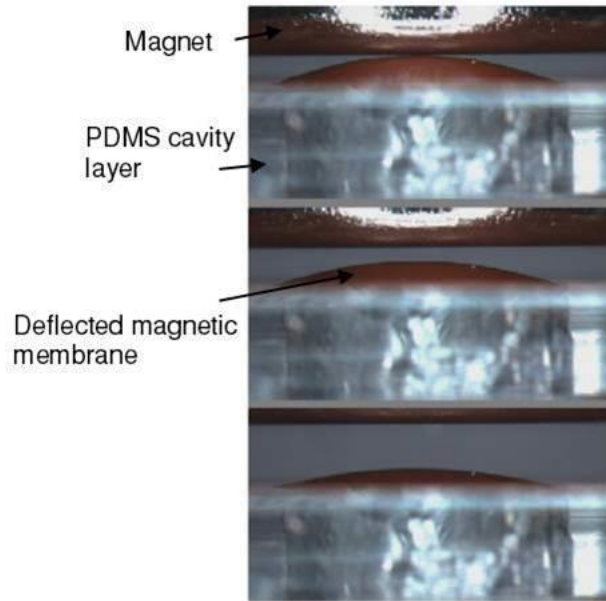


Figure 1.6: Membrane (7 mm in diameter and 35 mm in thickness, made of 40% w/w of magnetic particles in PDMS) deflection as a function of magnet position. The membrane shows a reduced deflection by increasing the magnet distance [68].

Even effective, the M-SSM shown in the second example is obtained by mixing solid (powder) magnetic additives with the host matrix. This strategy is prone to form aggregates to reduce the energy associated with the high surface area to volume ratio of the nano-sized particles. These heterogeneities are inducing non-homogeneous functionality on the material, which results in poor performance, as could be uneven mechanical properties of the M-SSM. An alternative is to disperse MNPs in carrier liquids [69]. Such stable colloidal form is generally known as ferrofluid (FF). In this context, G. Filipcsei *et al* [70], studied the cross-linked networks of elastomers swollen by FF. In response to an applied magnetic field, the obtained M-SSM changes its shape as a function of the magnetic field applied for a concentration of 20 wt% of FF, as it can be seen in Figure 1.7. Thus, for a magnetic field applied corresponding to 4 kG an elongation of 894 μm is obtained.

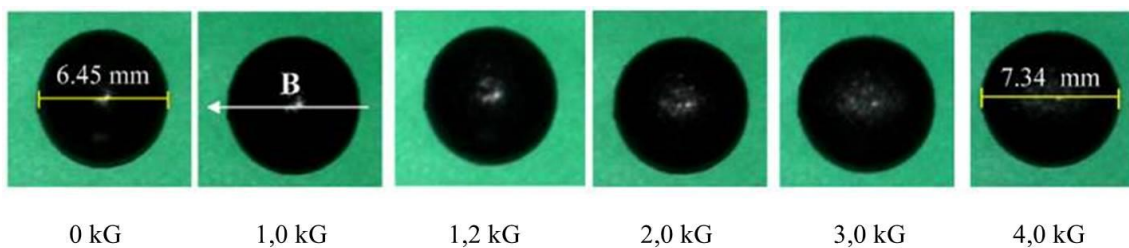


Figure 1.7: Dependence of a magnetic polymer on the magnetic field intensity. The concentration of the iron particles included in the ferrofluid are 20 wt% [70]. The arrow indicates the direction of the magnetic field, and the numbers below each image denote the magnetic field.

1. Introduction

Light sensitive materials

Although M-SSM have shown to have outstanding performance, they also present some limitations and drawbacks, being the most significant the small working distances in which either a magnet or a coil provides with enough magnetic actuation. For this reason the use of alternative contactless actuation methods are explored and developed. An interesting candidate is the use of light as external stimulus. Thus, a material generally known as light SSM (L-SSM) is achieved. Light can instantaneously deliver energy in specific amounts of intensity with high location accuracy [71]. Moreover, the use of light is attractive because of their own characteristics such as spatially, wavelength and intensity that can be varied quickly, easily, and remotely, enabling light to be one of the most controllable stimuli [72], [73]. Among the different dopants used in L-SSM, chromophores or nanoparticles are mostly used with the purpose to increase the absorption of the polymer at specific wavelengths, which finally results in a localized heating of the matrix and its subsequent volume variation. This is known as light-thermal process and it is based on the following physical principles: light absorbed by the dopants bring them to an energy excited state. Since most of them have an indirect bandgap, they undergo a non-radiative relaxation, in the form of the Joule effect. Due to the thermal conductivity of the dopants, the heat generated is transferred to the polymeric matrix, resulting in the actuation, mostly in the form of expansion of the bulk material. Although, the response time corresponding to light (or magnetic) actuation is longer as compared to the electrostatic case (1-3 ms vs 2-30 μ s, respectively) [74] their easily implementation on a system is attractive as compared to their electrostatic counterparts. The work presented by Y. Yu *et al* [75] is an example of a L-SSM having photosensible molecules (azobenzene) as dopants allowed a light-actuated MOEMS. The actuation (bending) is achieved in response to UV light, which induces a volume contraction in the surface region; see Figure 1.8(a). Concretely, a photoinduced bending is obtained in different directions in response to irradiation by linearly polarized light of different angles of polarization (represented white arrows in Figure 1.8(a)) at 366 nm, and bending is not observed again by visible light at > 540 nm. In another published work, C. L. Van Oosten, *et al*, an actuator based on using different wavelengths is presented [76]. Here, two strips of different polymers are glued together at one end (DR1A mounted at the top (red color) and A3MA (yellow color) mounted at the bottom), see Figure 1.8(b) (first left picture). Actuator responses at

1. Introduction

different wavelengths are shown in Figure 1.8(b). The resulting strip is actuated in air using light of different wavelengths obtaining responses such as: i) in the steady-state; ii) for a small bend at the top for a illumination of visible light (455 nm - 550 nm); iii) rapid and strong bending over the whole strip length when it is illuminated with a combination of ultraviolet and visible light and iv) a final state completely bent into the light with only ultraviolet illumination. With the light off, the film completely relaxes back to its original position.

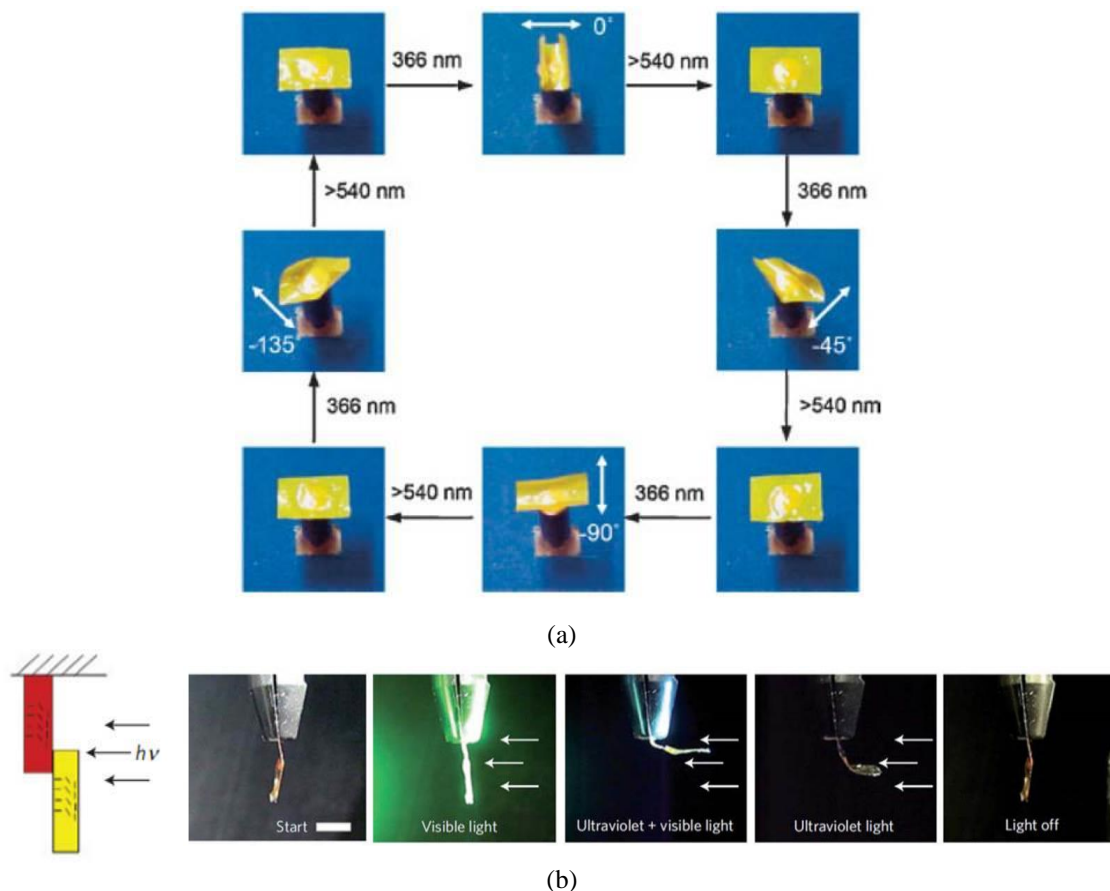


Figure 1.8: (a) Precise control of light bending direction of an LCE film by linearly polarized light. Photographic frames of the film bending in different directions in response to irradiation by linearly polarized light of different angles of polarization at 365 nm, and bending flattened again by visible light at > 540nm [75]. (b) Steady-state responses for a strip based on A3MA and DR1A polymers to different colours of light (scale bar 5 mm) [76].

Identical to the M-SSM previously discussed, the L-SSM suitable to provide shape changes requires polymers with low γ to assure a high flexibility. Additionally, they must have a coefficient of thermal expansion (CTE) significantly high so as to have efficient energy transference between the dopant and the polymeric matrix,

1. Introduction

allowing obtaining the desired actuation. Finally, in order to achieve high mechanical quality, the polymer must be able to be patterned with high aspect ratios. A polymer that has such properties is the well-known epoxy-based negative-tone polymer, SU-8. This photoresist has a Y ranging from 4.25 GPa to 4.95 GPa and a high coefficient of thermal expansion (CTE 52 ppm/°C) [77], as well as an outstanding high aspect ratio (up to 1:50). To date, SU-8 is applied into VOAs systems based on electro-thermal actuation [78] [79], Here, aluminium stripes are defined on top of SU-8 MOEMS and wire bonded to a power supply operating in DC: at 0.6 V the waveguides (located at the frame and at the seismic mass) are completely misaligned results in 20 dB attenuation with a power consumption of only 12 mW. The resistance of the stripes causes heat which is transferred to the polymeric matrix, achieving the actuation. Although effective, the response time is of some hundreds of milliseconds. In addition, the aluminium stripes may be detached from the SU-8 after several duty cycles, compromising the applicability.

Other polymer that has been used in this work is named Epocore [80]. This polymer presents much higher optical transparency than SU-8 with losses <0.2 dB/cm, at $\lambda = 850$ nm in the visible-NIR range [81]. After exposure to UV irradiation, aspect ratios higher than 10:1 are obtained. Among the main applications [80] of this material the optical applications in micro system technology [82] are highlighted. An example of this is the work presented by T. Guan et al [83]. Here, the Epocore is photopatterned obtaining a microlens with a tuneable focal length which is integrated on an optical platform. The focal length can be modulated by the absorption of a fluid (from 0.3 mm to 1 mm). Thereby the microlens acts as a light intensity modulator changing the transmitted intensity up to factor 8. Thus, such epoxy has potentials for optical applications in microfluidic channels, e.g. for bio/chemical sensing.

1. Introduction

Objectives addressed in this Thesis

Magnetic actuated polymers

Aiming towards contributing to this exciting field of research, in this Ph.D., ferrofluid (FF) is used in combination with polydimethylsiloxane (PDMS) obtaining a magnetic stimuli sensitive material (M-SSM). Even the combination of PDMS and FF results in an extremely promising M-SSM, its properties are seldomly reported and, to date, it is not applied to any micro-opto-electromechanical system (MOEMS). In this thesis, we aim to tackle this issue by characterizing M-SSMs obtained using PDMS as host matrix and isoparaffin-based FF containing Fe_3O_4 nanoparticles with diameter ranging between 3 nm and 15 nm [84] as additive. Additionally, different properties of the M-SSM as a function of FF concentration are here studied. Firstly, the internal structure of the M-SSM, i.e., the size particle, and distribution are analysed by transmission electron microscopy (TEM). Then, the M-SSM is both magnetic and optically characterized in bulk and mechanically characterized using cantilevers fabricated by soft lithography (SLT) [85]. Finally, a biocompatibility study of the M-SSM is carried out.

After the characterization of the M-SSM, it is applied for obtaining a VOA-MOEMS based on SLT. Concretely, two VOAs using either the M-SSM or the FF in combination with non-doped PDMS are presented. They have an identical waveguide cantilever with two-fold functions: i) to confine light (waveguiding); ii) and to be able to deflect in response to the application of an external stimulus.

More in detail, the design of those structures from the optical point of view consists on a waveguide-cantilever with two sets of air mirrors [86] distributed along the cantilever axis obtaining a Total Internal Reflection (TIR) waveguide. At the end of

1. Introduction

such structure a cylindrical microlens is defined which focuses the confined light on a collecting fiber optics. From the magnetic point of view, the design includes two reservoirs connected with a U-shaped microchannel that circumvents the waveguide-cantilever at its bottom section.

For implementing the magnetic material in these systems, two techniques are used: SLT and a combination between SLT and inkjet printing technique (IJP). For the SLT approach, the M-SSM fills the U-shaped microchannel, followed by the pouring of a non-doped PDMS over the first layer formed by M-SSM defining the bilayer system, Figure 1.9(a). The second proposed MOEMS is obtained by using IJP in combination with SLT. IJP allows dispensing a given amount of FF droplets on a non-cured PDMS structure previously defined by SLT. The FF droplets are entrapped with a second, non-doped PDMS, layer resulting in a MOEMS with the FF located in specific actuation areas, Figure 1.9(b). These MOEMS are mechanical and optical characterized and the results are discussed in the following section.

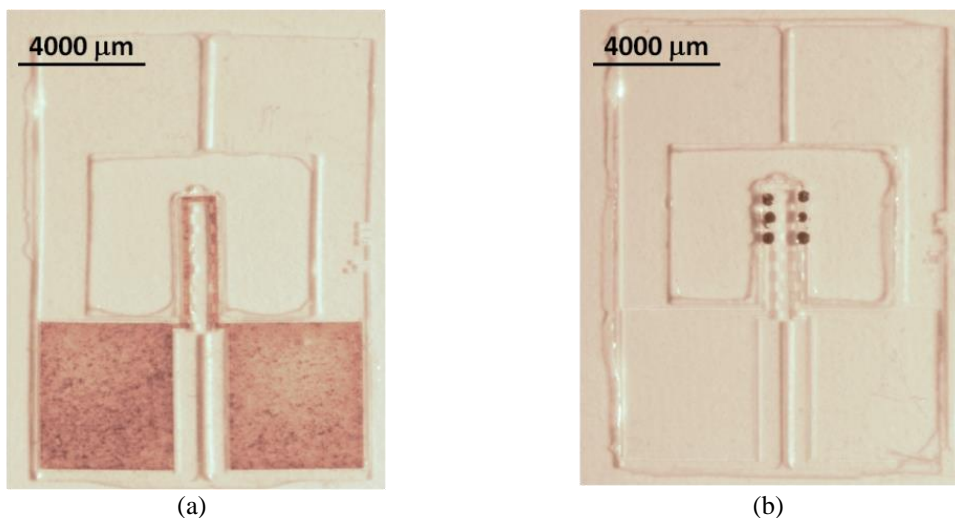


Figure 1.9: Real MOEMS images after fabrication process for (a) SLT and (b) IJP.

Light actuated polymers

In the second part of this thesis, optically-actuable VOA-MOEMS are defined using a light sensitive stimuli material L-SSM which is obtained with two different negative-tone photoresists: the Epocore and SU-8 as matrix and non-polar dyes as dopant obtaining what will be called hereafter L-SSM_{Ep0} and L-SSM_{SU-8}, respectively.

1. Introduction

Initially, the structurability of the L-SSM_{Epo} is verified by performing standard UV lithography and the results are compared with non-doped Epocore. Then, both L-SSM_{Epo} and L-SSM_{SU-8} are used to define optical test structures based in absorbance. In this configuration, for a fixed dye concentration and optical path, the absorbance at a specific wavelength can be determined, as it will also be discussed in the following section. Thus, key information regarding both dye concentration and required path length (dimensions of the actuation region) is obtained from such characterization which is applied to define an all-optical VOA-MOEMS. Its mechanical structure is a quad beam [87], consisting on one inertial mass and four external beams (springs). The design of the VOA-MOEMS developed in this thesis can be seen in Figure 1.10(a). When comparing both the quad beam and the cantilever with similar dimensions, it is known that the former presents lower mechanical sensitivity. However, it also has higher natural frequencies and, in addition, the mass displacement is equal in all the points of the mass due to the symmetry of the structure. Therefore, any structure on the mass (i.e. waveguides) has a horizontal displacement perpendicular to the system without any tilt. Optically the system consists of three waveguides which are defined on the VOA's seismic mass, playing the role of sensing elements. These waveguides are aligned to fish-bone shaped structures for appropriate fiber optics alignment and clamping. The L-SSM_{SU-8} is positioned in specific regions of the mechanical beams (hereafter named "actuation points"). The actuation is performed by directing specific wavelengths at the actuation points resulting in a strong absorption of the L-SSM_{SU-8} with an increase in the heating and, straightforwardly, an expansion of the color dye-doped SU-8. This entails a displacement of the seismic mass causing a misalignment (i.e. an increase of the optical losses) between the waveguide and the input/output fiber optics (as function of the power actuation, resulting on a light modulation coupled waveguide. Figure 1.10(b) shows, a real image of the fabricated VOA-MOEMS where the designed elements are observed. Moreover, the optical actuation elements which are defined by the L-SSM_{SU-8} and the rest of the structure by SU-8 can also be seen.

1. Introduction

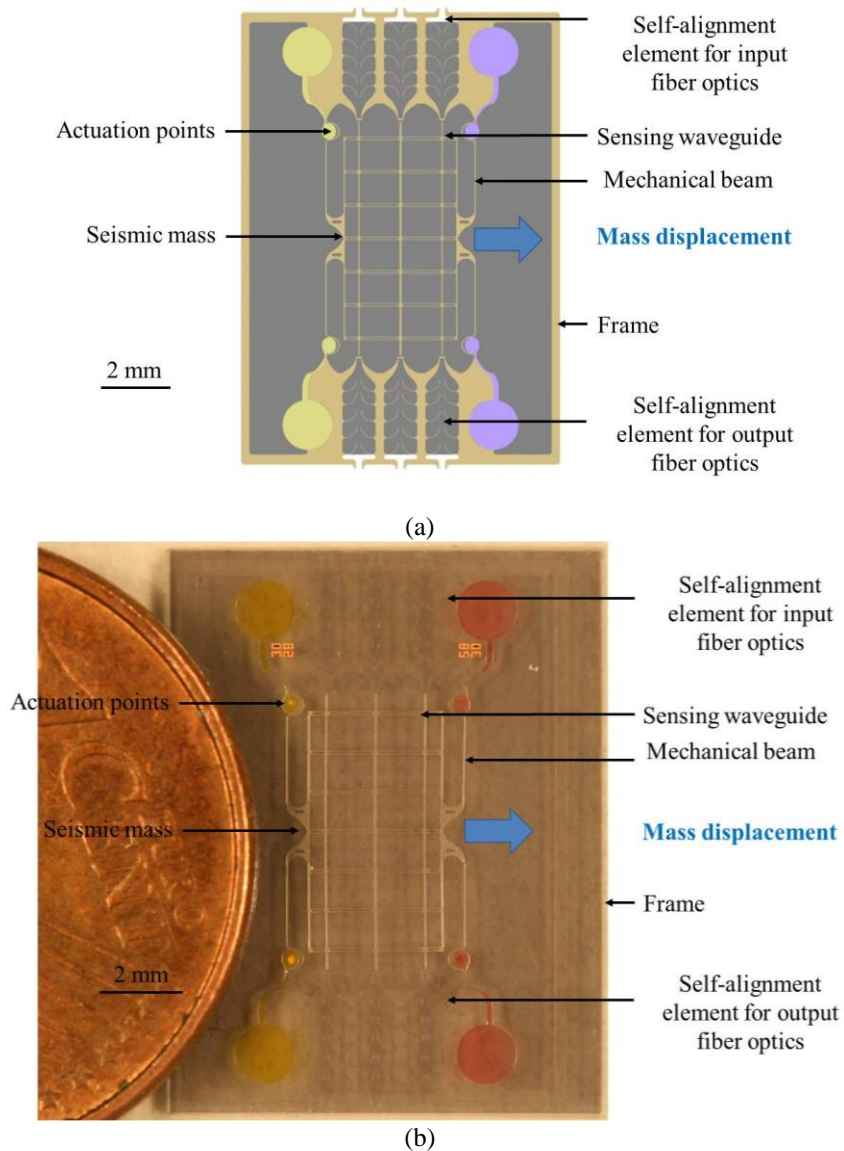


Figure 1.10: (a) Schematic view of the VOA-MOEMS with the main parts indicated: optical attenuation element, seismic mass, self-alignment structure and sensing waveguide. (b) A real image where the dye doped and undoped SU-8 are shown as well as the actuation points, mechanical beam, waveguide and self-alignment structure.

1. Introduction

REFERENCES

- [1] A. J. Padgaonkar, K. W. Krieger, and A. I. King, "Measurement of angular acceleration of a rigid body using linear accelerometers.," *Jouranl Appl. Mech. Trans. Am. Soc. Mech. Eng.*, no. 75, pp. 552–556, 1975.
- [2] R. . Grace and P. Salomon, "Making business with microsystems. Microsystems/MEMS/Micomachines on the move from technology to business.," *MST news, Int. Newsl. Microsystems MEMS*, vol. 5, pp. 4–8, 2001.
- [3] S. . Spearing, "Materials issues in microelectromechanical systems (MEMS)," *Acta Mater.*, vol. 48, no. 1, pp. 179–196, Jan. 2000.
- [4] M. E. Khater, M. Al-Ghamdi, S. Park, K. M. E. Stewart, E. M. Abdel-Rahman, A. Penlidis, A. H. Nayfeh, A. K. S. Abdel-Aziz, and M. Basha, "Binary MEMS gas sensors," *J. Micromechanics Microengineering*, vol. 24, no. 6, p. 065007, Jun. 2014.
- [5] R. R. Jivani, G. J. Lakhtaria, D. D. Patadiya, L. D. Patel, N. P. Jivani, and B. P. Jhala, "Biomedical microelectromechanical systems (BioMEMS): Revolution in drug delivery and analytical techniques," *Saudi Pharm. J.*, Dec. 2013.
- [6] I. Voiculescu and A. N. Nordin, "Acoustic wave based MEMS devices for biosensing applications.," *Biosens. Bioelectron.*, vol. 33, no. 1, pp. 1–9, Mar. 2012.
- [7] J. A. Plaza, A. Llobera, C. Dominguez, J. Esteve, I. Salinas, J. Garcia, and J. Berganzo, "BESOI-Based Integrated Optical Silicon Accelerometer," *J. Microelectromechanical Syst.*, vol. 13, no. 2, pp. 355–364, Apr. 2004.
- [8] S. J. Lee and D.-W. Cho, "Development of a micro-opto-mechanical accelerometer based on intensity modulation," *Microsyst. Technol.*, vol. 10, no. 2, pp. 147–154, Jan. 2004.
- [9] T. K. Gangopadhyay, "Prospects for Fibre Bragg Gratings and Fabry-Perot Interferometers in fibre-optic vibration sensing," *Sensors Actuators A Phys.*, vol. 113, no. 1, pp. 20–38, Jun. 2004.
- [10] F. A. Castro, S. R. M. Carneiro, O. Lisboa, and S. L. A. Carrara, "Two-mode optical fiber accelerometer," *Opt. Lett.*, vol. 17, no. 20, p. 1474, Oct. 1992.
- [11] S. J. Lukes and D. L. Dickensheets, "MEMS mirror for flexible z-axis control in a commercial confocal microscope," in *2012 International Conference on Optical MEMS and Nanophotonics*, 2012, pp. 148–149.
- [12] H. Choi, M. Choi, D. Shim, and S. H. Nam, "Optical MEMS and nanophotonics in Samsung Electronics," in *2013 International Conference on Optical MEMS and Nanophotonics (OMN)*, 2013, pp. 3–4.

1. Introduction

- [13] J. Chang, K.-D. Jung, E. Lee, M. Choi, S. Lee, and W. Kim, "Variable aperture controlled by microelectrofluidic iris.," *Opt. Lett.*, vol. 38, no. 15, pp. 2919–22, Aug. 2013.
- [14] P. Muller, R. Feuerstein, and H. Zappe, "A fully integrated optofluidic micro-iris," in *2012 IEEE 25th International Conference on Micro Electro Mechanical Systems (MEMS)*, 2012, pp. 7–10.
- [15] L. Li, C. Liu, H. Ren, and Q.-H. Wang, "Adaptive liquid iris based on electrowetting.," *Opt. Lett.*, vol. 38, no. 13, pp. 2336–8, Jul. 2013.
- [16] B. M. Kaylor, C. R. Wilson, N. J. Greenfield, P. A. Roos, E. M. Seger, M. J. Moghimi, and D. L. Dickensheets, "Miniature non-mechanical zoom camera using deformable MOEMS mirrors," in *Proceedings of SPIE - The International Society for Optical Engineering*, 2012, vol. 8252, p. 82520N.
- [17] P. Müller, A. Kloss, P. Liebetraut, W. Mönch, and H. Zappe, "A fully integrated optofluidic attenuator," *J. Micromechanics Microengineering*, vol. 21, no. 12, p. 125027, Dec. 2011.
- [18] H. Omran, Y. M. Sabry, M. Sadek, K. Hassan, M. Y. Shalaby, and D. Khalil, "MEMS optical tunable filter based on free-standing subwavelength silicon layers," in *Proceedings of SPIE - The International Society for Optical Engineering*, 2014, vol. 8977, p. 89770V.
- [19] M.-H. Jun, S. Moon, and J.-H. Lee, "Microassembly process to fabricate a microoptoelectromechanical systems scanning mirror with angular vertical comb electrodes," *J. Micro/Nanolithography, MEMS, MOEMS*, vol. 12, no. 1, p. 013006, Feb. 2013.
- [20] B. Reig, T. Camps, V. Bardinal, D. Bourrier, E. Daran, J. B. Doucet, J. Launay, and Fourniols J. Y., "Fabrication of polymer-based optical microsystem arrays suited for the active focusing of vertical laser diodes," *J. Micromechanics Microengineering*, vol. 22, pp. 1–6, 2012.
- [21] K. Zandi, J. Zou, B. Wong, R. V. Kruzelecky, and Y.-A. Peter, "VOA-based optical MEMS accelerometer," in *16th International Conference on Optical MEMS and Nanophotonics*, 2011, pp. 15–16.
- [22] M. Kristensen, K. Cook, and J. Canning, "Wavelength-selective mode-switching in a reflective long period grating mach-zehnder interferometer," in *Bragg Gratings, Photosensitivity, and Poling in Glass Waveguides, BGPP 2012*, 2013.
- [23] N. Weber, D. Hertkorn, H. Zappe, and A. Seifert, "Polymer/Silicon Hard Magnetic Micromirrors," *J. Microelectromechanical Syst.*, vol. 21, no. 5, pp. 1098–1106, Oct. 2012.
- [24] S. K. Y. Tang, C. A. Stan, and G. M. Whitesides, "Dynamically reconfigurable liquid-core liquid-cladding lens in a microfluidic channel.," *Lab Chip*, vol. 8, no. 3, pp. 395–401, Mar. 2008.

1. Introduction

- [25] B. Barber, C. R. Giles, V. Askyyuk, R. Ruel, L. Stulz, and D. Bishop, "A fiber connectorized MEMS variable optical attenuator," *IEEE Photonics Technol. Lett.*, vol. 10, no. 9, pp. 1262–1264, Sep. 1998.
- [26] H. Ren and E. Gerhard, "Design and fabrication of a current-pulse-excited bistable magnetic microactuator," *Sensors Actuators A Phys.*, vol. 58, no. 3, pp. 259–264, Mar. 1997.
- [27] H. J. Li, Y. J. Yang, J. J. Wang, Y. Q. Xu, Q. L. Zheng, and W. Y. Chen, "Low cost MEMS variable optical attenuator for optical telecommunication application," *Chinese J. Sensors Actuators*, vol. 19, no. 5, pp. 1731–1734, 2006.
- [28] X. Dai, "Micromachined electromagnetic variable optical attenuator for optical power equalization," *J. Micro/Nanolithography, MEMS, MOEMS*, vol. 4, no. 4, p. 041304, Oct. 2005.
- [29] N. A. Riza and S. Sumriddetchkajorn, "Digitally controlled fault-tolerant multiwavelength programmable fiber-optic attenuator using a two-dimensional digital micromirror device," *Opt. Lett.*, vol. 24, no. 5, pp. 282–284, 1999.
- [30] C. Marxer, C. Thio, M.-A. Gretillat, N. F. de Rooij, R. Battig, O. Anthamatten, B. Valk, and P. Vogel, "Vertical mirrors fabricated by deep reactive ion etching for fiber-optic switching applications," *J. Microelectromechanical Syst.*, vol. 6, no. 3, pp. 277–285, 1997.
- [31] C. R. Giles, V. Aksyyuk, B. Barber, R. Ruel, L. Stulz, and D. Bishop, "A silicon MEMS optical switch attenuator and its use in lightwave subsystems," *IEEE J. Sel. Top. Quantum Electron.*, vol. 5, no. 1, pp. 18–25, 1999.
- [32] Y. Liu, J. Xu, S. Zhong, L. Zhai, and Y. Wu, "Variable optical attenuator based on a vertical comb drive actuated MEMS micromirror," *Opt. - Int. J. Light Electron Opt.*, vol. 124, no. 20, pp. 4100–4103, Oct. 2013.
- [33] D. Kumar Agrawal and S. Bhattacharya, "Integrated optical and MEMS based design process for a variable optical attenuator," *Opt. Lasers Eng.*, vol. 49, no. 7, pp. 848–854, Jul. 2011.
- [34] Y. Liu, J. Xu, S. Zhong, L. Zhai, and Y. Wu, "Variable optical attenuator based on a vertical comb drive actuated MEMS micromirror," *Opt. - Int. J. Light Electron Opt.*, vol. 124, no. 20, pp. 4100–4103, Oct. 2013.
- [35] K.-Y. Lee, Y.-P. Yang, I.-C. Yang, Y.-L. Tsai, H.-F. Liao, Y.-J. Lin, W.-Y. Lee, and Y.-T. Tsai, "Optical logic operation for AND gate based on planar photonic crystal circuit," in *Proceedings of SPIE - The International Society for Optical Engineering*, 2011, vol. 8308, p. 83081S.
- [36] C.-L. Sun, Z.-B. Li, C.-T. Zheng, Q.-Q. Luo, X.-L. Huang, and D.-M. Zhang, "Low-voltage and compact polymeric optical switches using a Mach-Zehnder interferometer and N side-coupled electro-optic microrings," *Opt. Commun.*, vol. 331, pp. 251–261, Nov. 2014.

1. Introduction

- [37] A. V Krishnamoorthy, X. Zheng, D. Feng, J. Lexau, J. F. Buckwalter, H. D. Thacker, F. Liu, Y. Luo, E. Chang, P. Amberg, I. Shubin, S. S. Djordjevic, J. H. Lee, S. Lin, H. Liang, A. Abed, R. Shafiiha, K. Raj, R. Ho, M. Asghari, and J. E. Cunningham, "A low-power, high-speed, 9-channel germanium-silicon electro-absorption modulator array integrated with digital CMOS driver and wavelength multiplexer.," *Opt. Express*, vol. 22, no. 10, pp. 12289–95, May 2014.
- [38] M. Puyol, Í. Salinas, I. Garcés, F. Villuendas, A. Llobera, C. Domínguez, and J. Alonso, "Improved Integrated Waveguide Absorbance Optodes for Ion-Selective Sensing," *Anal. Chem.*, vol. 74, no. 14, pp. 3354–3361, Jul. 2002.
- [39] E. A. Kane, M. Gershow, B. Afonso, I. Larderet, M. Klein, A. R. Carter, B. L. de Bivort, S. G. Sprecher, and A. D. T. Samuel, "Sensorimotor structure of *Drosophila* larva phototaxis.," *Proc. Natl. Acad. Sci. U. S. A.*, vol. 110, no. 40, pp. E3868–77, Oct. 2013.
- [40] J. J. Brandner, "Microfabrication in metals, ceramics and polymers," *Russ. J. Gen. Chem.*, vol. 82, no. 12, pp. 2025–2033, Jan. 2013.
- [41] C. Liu, "Recent Developments in Polymer MEMS," *Adv. Mater.*, vol. 19, no. 22, pp. 3783–3790, Nov. 2007.
- [42] G. Pasparakis and M. Vamvakaki, "Multiresponsive polymers: nano-sized assemblies, stimuli-sensitive gels and smart surfaces," *Polym. Chem.*, vol. 2, no. 6, p. 1234, May 2011.
- [43] D. Roy, J. N. Cambre, and B. S. Sumerlin, "Future perspectives and recent advances in stimuli-responsive materials," *Prog. Polym. Sci.*, vol. 35, no. 1–2, pp. 278–301, Jan. 2010.
- [44] S. Dai, P. Ravi, and K. C. Tam, "pH-Responsive polymers: synthesis, properties and applications," *Soft Matter*, vol. 4, no. 3, p. 435, Feb. 2008.
- [45] S. Dai, P. Ravi, and K. C. Tam, "Thermo- and photo-responsive polymeric systems," *Soft Matter*, vol. 5, no. 13, pp. 2513–2533, Jun. 2009.
- [46] R. Shankar, T. K. Ghosh, and R. J. Spontak, "Dielectric elastomers as next-generation polymeric actuators," *Soft Matter*, vol. 3, no. 9, p. 1116, Aug. 2007.
- [47] T. Kimura, Y. Umehara, and F. Kimura, "Magnetic field responsive silicone elastomer loaded with short steel wires having orientation distribution," *Soft Matter*, vol. 8, no. 23, p. 6206, May 2012.
- [48] F. Liu and M. W. Urban, "Recent advances and challenges in designing stimuli-responsive polymers," *Prog. Polym. Sci.*, vol. 35, no. 1–2, pp. 3–23, Jan. 2010.
- [49] G. Filipcsei, I. Csetneki, A. Szilágyi, and M. Zrínyi, "Magnetic field-responsive smart polymer composites," *Adv. Polym. Sci.*, vol. 206, no. 1, pp. 137–189, 2007.

1. Introduction

- [50] Y. Qiu and K. Park, "Environment-sensitive hydrogels for drug delivery," *Adv. Drug Deliv. Rev.*, vol. 64, no. SUPPL., pp. 49–60, Dec. 2012.
- [51] H. Y. Jiang, S. Kelch, and A. Lendlein, "Polymers Move in Response to Light," *Adv. Mater.*, vol. 18, no. 11, pp. 1471–1475, Jun. 2006.
- [52] M. A. Ward and T. K. Georgiou, "Thermoresponsive Polymers for Biomedical Applications," *Polymers (Basel)*, vol. 3, no. 4, pp. 1215–1242, Aug. 2011.
- [53] "No Title." [Online]. Available: <http://www.mit.edu/~6.777/matprops/pdms.htm>.
- [54] Y. H. Ko, S. H. Lee, J. W. Leem, and J. S. Yu, "High transparency and triboelectric charge generation properties of nano-patterned PDMS," *RSC Adv.*, vol. 4, no. 20, p. 10216, 2014.
- [55] B. Ibarlucea, C. Díez-Gil, I. Ratera, J. Veciana, A. Caballero, F. Zapata, A. Tárraga, P. Molina, S. Demming, S. Büttgenbach, C. Fernández-Sánchez, and A. Llobera, "PDMS based photonic lab-on-a-chip for the selective optical detection of heavy metal ions.," *Analyst*, vol. 138, no. 3, pp. 839–44, Feb. 2013.
- [56] M. Ionescu, B. Winton, D. Wexler, R. Siegele, A. Deslantes, E. Stelcer, A. Atanacio, and D. D. Cohen, "Enhanced biocompatibility of PDMS (polydimethylsiloxane) polymer films by ion irradiation," *Nucl. Instruments Methods Phys. Res. Sect. B Beam Interact. with Mater. Atoms*, vol. 273, no. null, pp. 161–163, Feb. 2012.
- [57] P. Song, D. J. H. Tng, R. Hu, G. Lin, E. Meng, and K.-T. Yong, "An electrochemically actuated MEMS device for individualized drug delivery: an in vitro study.," *Adv. Healthc. Mater.*, vol. 2, no. 8, pp. 1170–8, Aug. 2013.
- [58] I. Yilgor and E. Yilgor, "Thermal stabilities of end groups in hydroxyalkyl terminated polydimethylsiloxane oligomers," *Polym. Bull.*, vol. 40, no. 4–5, pp. 525–532, Apr. 1998.
- [59] D. Kim and K.-S. Yun, "Patterning of carbon nanotube films on PDMS using SU-8 microstructures," *Microsyst. Technol.*, vol. 19, no. 5, pp. 743–748, Oct. 2012.
- [60] H. Makamba, J. H. Kim, K. Lim, N. Park, and J. H. Hahn, "Surface modification of poly(dimethylsiloxane) microchannels.," *Electrophoresis*, vol. 24, no. 21, pp. 3607–19, Nov. 2003.
- [61] S. R. Sershen, G. A. Mensing, M. Ng, N. J. Halas, D. J. Beebe, and J. L. West, "Independent Optical Control of Microfluidic Valves Formed from Optomechanically Responsive Nanocomposite Hydrogels," *Adv. Mater.*, vol. 17, no. 11, pp. 1366–1368, Jun. 2005.
- [62] G. Filipcsei, J. Fehér, and M. Zrínyi, "Electric field sensitive neutral polymer gels," *J. Mol. Struct.*, vol. 554, no. 1, pp. 109–117, Oct. 2000.

1. Introduction

- [63] M. Khoo and C. Liu, "Micro magnetic silicone elastomer membrane actuator," *Sensors Actuators A Phys.*, vol. 89, no. 3, pp. 259–266, Apr. 2001.
- [64] A. Singh, M. Shirolkar, M. V. Limaye, S. Gokhale, C. Khan-Malek, and S. K. Kulkarni, "A magnetic nano-composite soft polymeric membrane," *Microsyst. Technol.*, vol. 19, no. 3, pp. 409–418, Aug. 2012.
- [65] D. Ivaneyko, V. Toshchevikov, M. Saphiannikova, and G. Heinrich, "Effects of particle distribution on mechanical properties of magneto-sensitive elastomers in a homogeneous magnetic field," Oct. 2012.
- [66] Q. A. Pankhurst, J. Connolly, S. K. Jones, and J. Dobson, "Applications of magnetic nanoparticles in biomedicine," *J. Phys. D. Appl. Phys.*, vol. 36, no. 13, pp. R167–R181, Jul. 2003.
- [67] F. N. Pirmoradi, J. K. Jackson, H. M. Burt, and M. Chiao, "A magnetically controlled MEMS device for drug delivery: design, fabrication, and testing.," *Lab Chip*, vol. 11, no. 18, pp. 3072–80, Sep. 2011.
- [68] F. Pirmoradi, L. Cheng, and M. Chiao, "A magnetic poly(dimethylsiloxane) composite membrane incorporated with uniformly dispersed, coated iron oxide nanoparticles," *J. Micromechanics Microengineering*, vol. 20, no. 1, p. 015032, Jan. 2010.
- [69] R. P. Castillejos, J. E. i Tintó, and J. A. P. Plaza, *Study and applications of ferrofluids in microfluidics*. Barcelona: Universitat Politècnica de Catalunya (UPC), Departament d'enginyeria Electrònica, 2003.
- [70] G. Filipcsei and M. Zrínyi, "Magnetodeformation effects and the swelling of ferrogels in a uniform magnetic field.," *J. Phys. Condens. Matter*, vol. 22, no. 27, p. 276001, Jul. 2010.
- [71] P. Bawa, V. Pillay, Y. E. Choonara, and L. C. du Toit, "Stimuli-responsive polymers and their applications in drug delivery.," *Biomed. Mater.*, vol. 4, no. 2, p. 022001, Apr. 2009.
- [72] E. M. White, J. Yatvin, J. B. Grubbs, J. A. Bilbrey, and J. Locklin, "Advances in smart materials: Stimuli-responsive hydrogel thin films," *J. Polym. Sci. Part B Polym. Phys.*, vol. 51, no. 14, pp. 1084–1099, Jul. 2013.
- [73] F. D. Jochum and P. Theato, "Temperature- and light-responsive smart polymer materials.," *Chem. Soc. Rev.*, vol. 42, no. 17, pp. 7468–83, Sep. 2013.
- [74] G. M. Rebeiz, "RF MEMS switches: status of the technology," in *TRansducers 2003, The 12th International Conference on Solid State Sensors, Actuators and Microsystems, Boston*, 2003, pp. 1726–1729.
- [75] Y. Yu and T. Ikeda, "Photodeformable Polymers: A New Kind of Promising Smart Material for Micro- and Nano-Applications," *Macromol. Chem. Phys.*, vol. 206, no. 17, pp. 1705–1708, Sep. 2005.

1. Introduction

- [76] C. L. van Oosten, C. W. M. Bastiaansen, and D. J. Broer, “Printed artificial cilia from liquid-crystal network actuators modularly driven by light.,” *Nat. Mater.*, vol. 8, no. 8, pp. 677–82, Aug. 2009.
- [77] H. Lorenz, M. Laudon, and P. Renaud, “Mechanical characterization of a new high-aspect-ratio near UV-photoresist,” *Microelectron. Eng.*, vol. 41–42, pp. 371–374, 1998.
- [78] A. Llobera, G. Villanueva, V. J. Cadarso, S. Battgenbach, and J. A. Plaza, “Polymeric MOEMS Variable Optical Attenuator,” *IEEE Photonics Technol. Lett.*, vol. 18, no. 22, pp. 2425–2427, Nov. 2006.
- [79] V. J. Cadarso, “Non conventional technologies for integrated optics,” Universitat Autònoma de Barcelona (UAB), 2008.
- [80] “<http://www.microresist.de>.” .
- [81] V. J. Cadarso, K. Pfeiffer, U. Ostrzinski, J. B. Bureau, G. A. Racine, A. Voigt, G. Gruetzner, and J. Brugger, “Direct writing laser of high aspect ratio epoxy microstructures,” *J. Micromechanics Microengineering*, vol. 21, no. 1, p. 017003, Jan. 2011.
- [82] A. Llobera, V. Seidemann, J. A. Plaza, V. J. Cadarso, and S. Buttgenbach, “SU-8 Optical Accelerometers,” *J. Microelectromechanical Syst.*, vol. 16, no. 1, pp. 111–121, Feb. 2007.
- [83] T. Guan, F. Ceysens, and R. Puers, “Tunable hydrogel microlens with built-in polymer waveguide and fiber clamp for MEMS applications,” in *2013 Transducers & Eurosensors XXVII: The 17th International Conference on Solid-State Sensors, Actuators and Microsystems (TRANSDUCERS & EUROSENSORS XXVII)*, 2013, pp. 522–525.
- [84] S. Odenbach, “Ferrofluids—magnetically controlled suspensions,” *Colloids Surfaces A Physicochem. Eng. Asp.*, vol. 217, no. 1–3, pp. 171–178, Apr. 2003.
- [85] Y. Xia and G. M. Whitesides, “Soft Lithography,” *Angew. Chemie Int. Ed.*, vol. 37, no. 5, pp. 550–575, Mar. 1998.
- [86] J. Vila-Planas, E. Fernández-Rosas, B. Ibarlucea, S. Demming, C. Nogués, J. A. Plaza, C. Domínguez, S. Büttgenbach, and A. Llobera, “Cell analysis using a multiple internal reflection photonic lab-on-a-chip.,” *Nat. Protoc.*, vol. 6, no. 10, pp. 1642–55, Oct. 2011.
- [87] T. Tschan, N. de Rooij, and A. Bezing, “Analytical and FEM modelling of piezoresistive silicon accelerometers: predictions and limitations compared to experiments,” *Sensors Mater.*, vol. 4, pp. 189–203, 1992.

2. Results & Discussion

2.1. Magnetic-sensitive stimuli material

The synthesis and characterization of the magnetic sensitive stimuli material (M-SSM) as a function of ferrofluid (FF) concentration is here presented. Firstly, the internal structure of the M-SSM (i.e., the size particle, the presence of aggregate the homogeneity) has been studied by transmission electron microscopy (TEM) analysis. Then, the M-SSM has been both magnetic and optically characterized using samples in bulk. The mechanical properties have also been obtained using cantilevers. Finally, the biocompatibility study of the M-SSM has been carried out. Such M-SSM has been implemented on magnetic variable optical attenuator-micro-opto-electro-mechanical system (VOA-MOEMS) with two different techniques i) soft lithography (SLT) and ii) inkjet printing technique (IJP).

2.1.1. *Magnetic-sensitive stimuli material synthesis*

M-SSM has been synthesized using PDMS as host matrix and isoparaffin-based FF containing Fe_3O_4 nanoparticles with size distribution of 10 nm as additive. First, the PDMS pre-polymer is obtained in a 1:10 (v:v) curing agent/base elastomer. Just afterwards, different weights per cent of FF are used (0, 4.6, 6.5, 14.9, 22.8, 29.9 and 35.8 in wt% FF) and manually stirred until homogeneous dispersion is achieved. The resulting M-SSMs are labelled as S_i ($i = 0, 1, \dots, 6$; corresponding to the increasing FF concentrations).

2. Results & Discussion

2.1.2. *Magnetic-sensitive stimuli material characterization*

After the M-SSM synthesis the characterization of M-SSM has been performed to obtain the physical properties and the biocompatibility of the development M-SSM as a function of FF concentration.

Polymerization

One of the most important issues when using PDMS in combination of an additive is to verify that the polymerization of the former is not affected by the presence of the latter. To this effect, S₀ to S₆ samples have been studied with the purpose of setting the upper threshold regarding the maximal FF concentration that can host the polymeric matrix, since incomplete polymerization may lead to fragile or brittle systems with a large variation of their properties (especially Young's modulus).

First evidence that upper threshold FF concentration can be found in the different required curing times. Longer polymerization times may be the evidence that the 3D crosslinking demands higher amount of energy to be achieved. In the synthesis corresponding to sample S₀ (0 wt% FF) 20 minutes at 80°C have been required for completing the polymerization time. These values have been used as reference. The same polymerization time has been needed with samples S₁ to S₃. Thus, the additive does not affect the formation of the 3D polymeric matrix. For samples S₄ and S₅ the curing time had to be increased to 25 minutes and up to 35 min for sample S₆. Although it has been possible to cure this last sample, such an increase of time required to achieve polymerization is significative and variations on the polymer structural properties should be expected. For this reason no higher concentrations above those used with S₆ have been considered.

Nanoparticles distribution

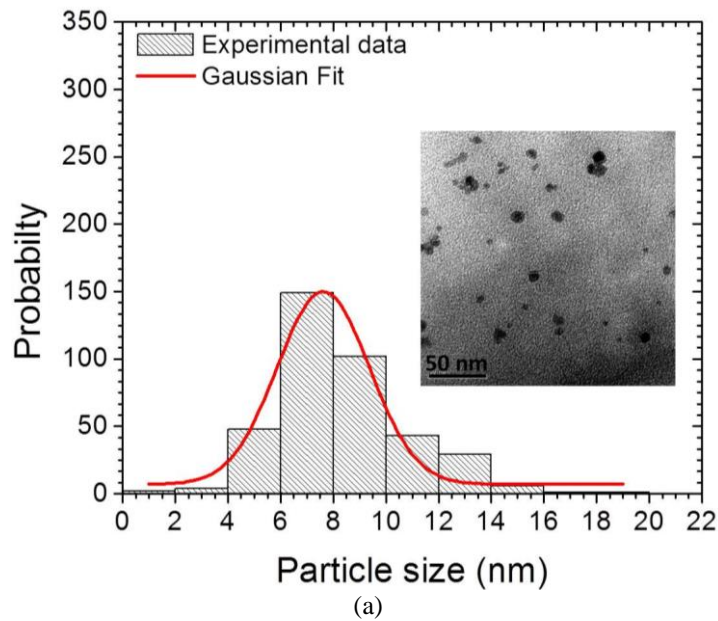
The internal structure of the M-SSM, i.e., the size particle, the aggregate formation and the homogeneous distribution has been studied for S₂ and S₆ by TEM. These two have been considered as examples of low and high FF concentration. This study has shown the absence of aggregates and the homogenous magnetic nanoparticles (MNP) distribution on the polymeric matrix regardless of the additive concentration. With TEM image analysis the nanoparticle size distribution has been obtained, (Table

2. Results & Discussion

2.1). Moreover, Figure 2.1. shows a Gaussian distribution corresponding to the values obtained from TEM analysis. This probability theory defines that such distribution is very common on continuous probability distribution. Thus, from the obtained nanoparticle size, named as D_{TEM} , and values corresponding for each studied samples $D_{\text{TEM}}(S_2) = 8 \pm 4$ nm, $D_{\text{TEM}}(S_6) = 7 \pm 4$ nm, it can be confirmed that PDMS matrix has been able to host much larger FF volumes and without the presence of aggregate size and number than in previously reported works [1]–[4]. In turn, this higher FF concentration should provide a higher actuation to a magnetic stimulus.

Table 2.1. Summary for values of nanoparticle size obtaining from TEM study (D_{TEM}).

Sample	D_{TEM} (nm)
S_2	8 ± 4
S_6	7 ± 4



2. Results & Discussion

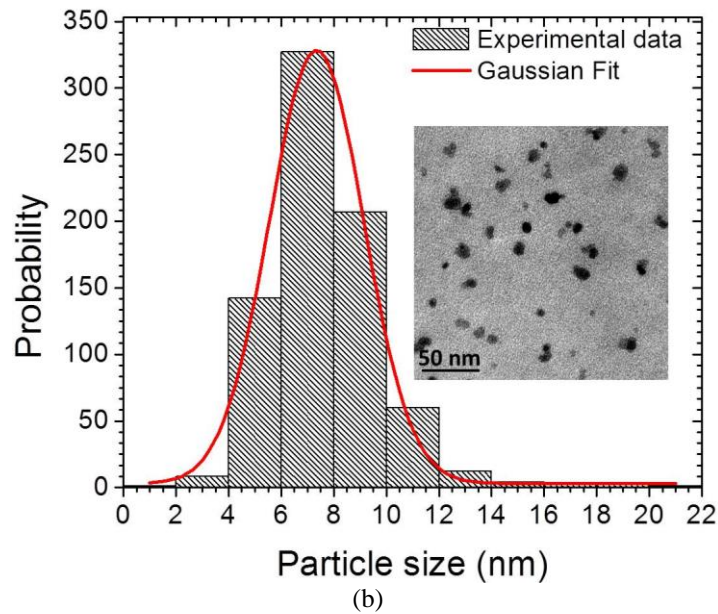


Figure 2.1: Nanoparticle size distribution by TEM image analysis and the Gaussian fitting (D_{TEM}) for (a) 6,5 wt% (S_2) and (b) 35.8 wt% (S_6) M-SSM. Caption A and B correspond to TEM images of both materials after polymerization, where the black scale bar corresponds to 50 nm.

Magnetization

The magnetization of slab samples from S_1 to S_6 at 300 K has been obtained using a vibrating sample magnetometer (VSM, Oxford Instruments, UK). Moreover, from this study the nanoparticle size could be determined and compared with the results presented in the TEM section.

The magnetic nature of the samples has been studied by measuring the magnetization as a function of the applied magnetic field. None of them show either coercivity or remanence at room temperature indicating a superparamagnetic behavior. This is in agree with the superparamagnetic nature of the 10 nm to 15 nm Fe_3O_4 nanoparticles embedded in the PDMS matrix [5], see Figure 2.2.

2. Results & Discussion

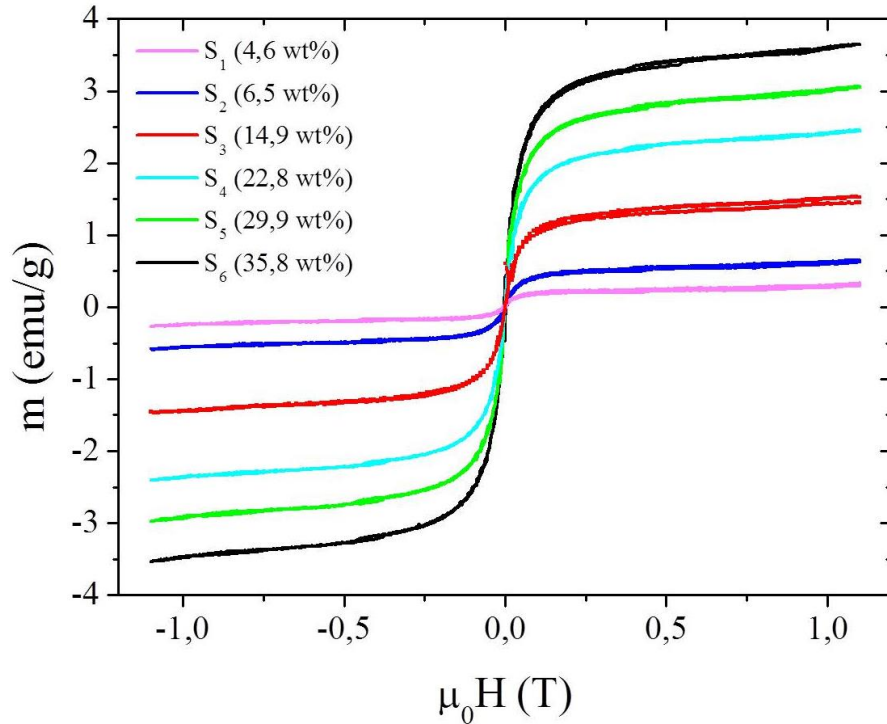


Figure 2.2: Magnetic loops for samples S_1 to S_6 at room temperature.

Furthermore the study of the magnetic particle size has been calculated using the Langevin [6] function:

$$m = m_S \left(\coth \left(\frac{\mu H}{k_B T} \right) - \frac{k_B T}{\mu H} \right) \quad (1)$$

where k_B is the Boltzmann constant, T is the absolute temperature, m_S is the saturation magnetization, H is the magnetic field, μ , is the true magnetic moment which is defined as

$$\mu = m_S \pi D_L^3 / 6 \quad (2)$$

where D_L is the magnetic particle size (obtaining from using Langevin function). First, m_S is calculated, from which analytical D_L values are obtained, which are compared with those from TEM study (D_{TEM}). This study was performed for samples S_2 and S_6 , and the results are summarized in Table 2.2. Differences between them are due to the fact that magnetic measurements do not take into account the presence of the surfactant layer [6] at the surface of the MNPs. Thus, the average values of D_L were smaller than D_{TEM} . The particle size has been recalculated including the thickness of a unit cell that corresponds to $a_0 = 0.83$ nm for magnetite [7], [8]. For spherical particles, introducing this correction into the Langevin function leads to the following expression:

2. Results & Discussion

$$D_L = D'_L - 2a_0 \quad (3) D'_L = \sqrt[3]{\frac{6\mu}{m_S\pi}} + a_0$$

where D'_L is the particle size considering both the magnetic particle size (D_L) and a_0 the unit cell correction, Eq. 3. Once this aspect is considered, a good agreement is obtained then between the D'_L value from Eq. 3 and TEM measurements (Table 2.2). On the basis of such results, it can be confirmed that no aggregates were formed in the M-SSM, even with the samples with the highest FF concentration.

Table 2.2. Summary for values of nanoparticle size obtaining from TEM study (D_{TEM}), from Eq. 2 (D_L), and Eq. 3 (D'_L) for both slab samples S_2 and S_6 .

Sample	D_{TEM} (nm)	D'_L (nm)	D_L (nm)
S_2	8 ± 4	8 ± 1	6 ± 1
S_6	7 ± 4	6 ± 1	4 ± 1

Biocompatibility

PDMS is known to be a compatible material with low or no toxicity [9], making it suitable to be used with samples of biological origin (cells, enzymes, bacteria, etc.). The study of biocompatibility of the developed M-SSM has been carried out for verifying whether the inclusion of FF in the PDMS alters the low or no toxicity of the polymeric matrix. The cytotoxicity, or what is known by the name of cell viability, is a common method to estimate biocompatibility of materials. Here, samples from S_0 to S_6 with three different slab geometries ($a=[w$ (width); l (length); h (height)] in mm) $a_1=[2; 5; 2]$; $a_2=[3; 5; 2]$; $a_3=[4; 5; 2]$ and corresponding volumes of $a_1=20\text{ mm}^3$; $a_2=30\text{mm}^3$ and $a_3=40\text{mm}^3$ were subjected to cytotoxicity study. The cytotoxicity has been determined using vascular smooth muscle cells (VSMC) cultured from rat aorta in combination with the magnetic samples (introduced into the wells where the experiment was conducted) by using the colorimetric MTT (3-(4,5-dimethylthiazol-2-yl)-2,5-diphenyltetrazolium bromide) assay [10]. This technique is based on the ability of viable cells to transform the MTT salt into formazan dyes. After a 24 h incubation period for VSMC which have been exposed to different quantities of M-SSM the polymer and the medium containing the samples have been aspirated, the wells have been washed with phosphate buffered solution and the MTT solution (1 mg/ml) has been added and incubates for 4 h. The purple formazan generated by viable cells has been solubilized with 20% sodium dodecyl sulphate in 0.02 M HCl and incubated for 10 h at 37°C. The optical density of each well has been determined at 540 nm in a

2. Results & Discussion

microplate spectrophotometer reader (BioTek® Synergy HT). Cell viability has been expressed as percentage in relation to controls (non-treated cells).

Thus, the cell viability as a function of the FF concentration has been obtained, Figure 2.3. Samples from S_0 to S_5 showed 100 % viability independently on the sample volume, i.e., those samples have presented low toxicity for all volumes and concentration of FF. On the contrary, for samples corresponding to the highest FF concentration (S_6) and for volume a_3 , the toxicity drastically increased as compared to the rest of the samples, i.e. the % cell viability decreased from $(120 \pm 4)\%$ to $(20 \pm 12)\%$. Thus, M-SSM presents low cytotoxicity and most of the prepared materials can be used in biological applications without additional modification.

It is necessary to clarify the results obtained with this technique: as control, cells are incubated with the medium only. If M-SSM shows no toxicity at certain concentrations, the viability could be exceeded of 100% (being 100% the viability control). Such exceed, could be caused by natural variations on the cellular metabolism or because the M-SSM has an influence on the cells.

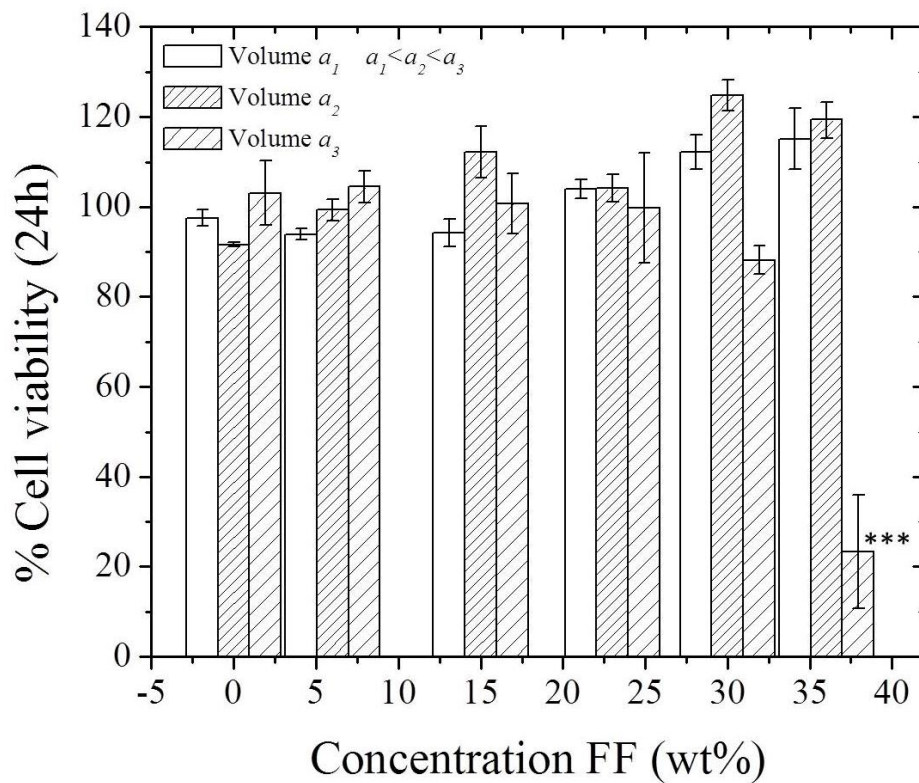


Figure 2.3: % Cell viability for different concentration of FF into the PDMS matrix and three volumes samples a_1 , a_2 and a_3 (20 mm^3 ; 30 mm^3 and 40 mm^3 , respectively). *** are the standard nomenclature in biological analysis to show a sharp variation in the tendency.

2. Results & Discussion

Mechanical properties

The Young's modulus of the M-SSM (Y_{M-SSM}) samples has been experimentally measured to study the stiffness of the host polymeric matrix as a function of the FF concentration. Thus, samples from S_1 to S_6 has been microstructured in the shape of cantilevers with 4400 μm lengths (Inset Figure 2.4) to quantify, for a fixed stimulus, their relative deflections. A confocal microscope (PL μ 2300 Optical Imaging Profiler, Sensofar, Spain) with software (Pl μ Confocal Imaging Profiler, Sensofar, Spain) has been used for determining the Y_{M-SSM} experimentally by recording deflections of the cantilevers under the action of the gravity. Y_{M-SSM} has been calculating using equation 4, where ρ is the M-SSM density, g the gravitational field, l the length and h the thickness of the cantilever and y_{max} the maximum deflection under the action of the gravitational field.

$$Y_{M-SSM} = \frac{3\rho gl^4}{2y_{max}h^2} \quad (4)$$

It should be emphasized that samples corresponding to the lowest FF concentration, i. e. S_1 and S_2 , presented very low contrast, impeding the characterization. To compensate this issue 2.5 mg of blue dye has been used to enhance the contrast. The experimental Y_{M-SSM} values corresponding for samples S_1 to S_6 as a function of the wt% of FF in the M-SSM are shown in Figure 2.4 (black squares). An increasing tendency of the Y_{M-SSM} has been observed for concentrations up to 29.9 wt % FF, then for a concentration of 35.8 wt% FF an abrupt decrease close to 30% is shown in Figure 2.4. This can be associated to the incomplete polymerization for FF concentration above 29.9 wt% FF.

The experimental results have been compared with a theoretical model [11]. It states that the Young's modulus of a composite based on rigid particles embedded in an elastic matrix (Y_{M-SSM} in our case) can be obtained from the Young's modulus of the unfilled polymer matrix (Y_{PDMS}) and a factor related to the amount of additives incorporated into the matrix. Thus, in a previous work from Rault *et al.*, [12], it has been shown that elastomers filled with solid particles present a quadratic modification of the Young's modulus, following:

2. Results & Discussion

$$Y_{M-SSM} = Y_{PDMS}(1 + 2.5C + 14.1C^2) \quad (5)$$

where, C is the volume fraction of the fillers in the PDMS ($C < 0.3$ in most studies) considering a system of rigid spheres interacting in a fluid. The obtained theoretical results has been presented in Figure 2.4 (red line), showing for moderate amount of fillers ($<20\%$) that Y_{M-SSM} is well approximated by a quadratic expression of volume fraction filler [13]. The measured results and the theoretical values of Y_{M-SSM} for S_6 did follow the predicted the quadratic tendency. The reason for this fact could be associated to the incomplete polymerization.

It must be specified that S_0 shows no experimental value because the mechanical study here presented corresponds to M-SSM samples. Nevertheless, the value of Y_{PDMS} corresponds to 360-870 kPa according to data sheet. This value for this study is for reference only because the dimensions/geometry of the structure that is attributed this value is not detailed. Moreover, considering the experimental errors the presented experimental data are in the range of the Young's modulus presented in the data sheet.

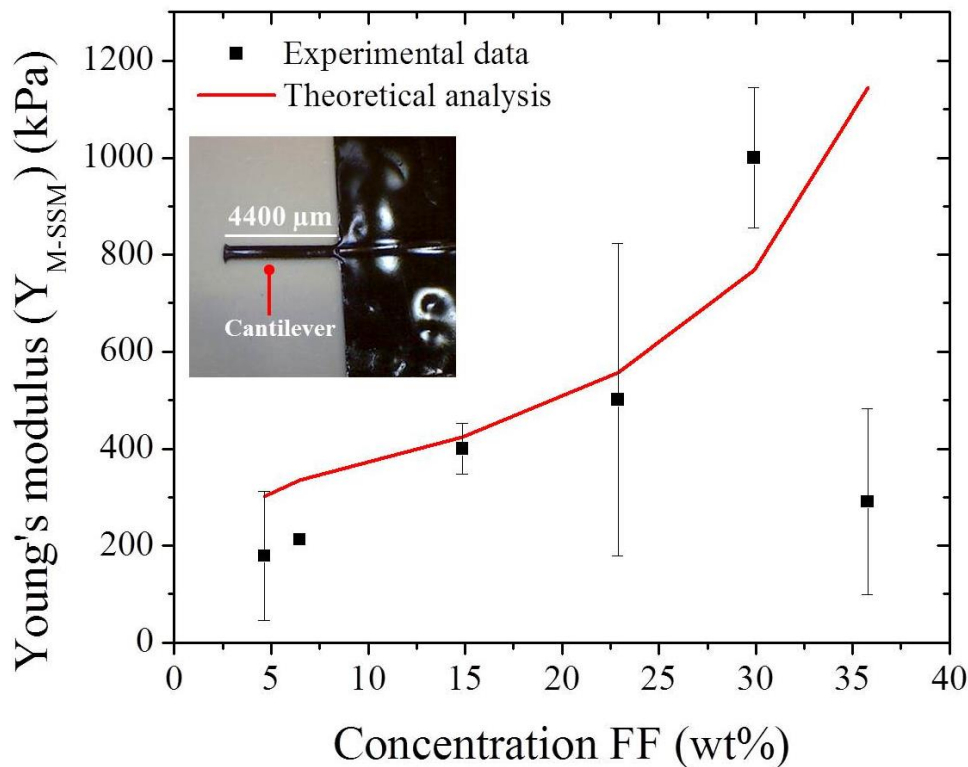


Figure 2.4: Magnetic-sensitive stimuli material Young's modulus (Y_{M-SSM}) for different ferrofluid (FF) concentrations (4.6, 6.5, 14.9, 22.8, 29.9 and 35.8 wt% FF). In red line the theoretical Y_{M-SSM} analysis is shown and in black squares the experimental data.

2. Results & Discussion

Optical properties

Optical properties of a polymeric matrix may strongly vary when additives are included. Thus, a transmittance (T) study as a function of the FF concentration has been carried out to determine the effect of the FF concentration on the M-SSM. When combining FF and PDMS, the optical and chemical properties of the liquid carrier may potentially change the spectral response of the M-SSM.

Results have shown how the transmittance of M-SSM decreased as the FF concentration increases, see Figure 2.5. Samples S_1 and S_2 had a decrease in transmittance below 50% (3 dB) and therefore, for optical path small enough, these M-SSM may still valid for developing photonic lab on a chip with magnetic actuation. Conversely, samples with larger FF concentration from S_3 to S_6 , have been considered as opaque in the working range since the decrease in transmittance has been higher than 73%. Even though they may have a higher displacement upon magnetic actuation, their high absorption impedes its direct use in MOEMS. A possibility to take advantage of such properties is to develop MOEMS in which both highly doped M-SSM (S_3 to S_6) are combined with other materials, such as non-doped PDMS. When using the adequate fabrication techniques such as soft lithography (SLT) or inkjet printing (IJP), it becomes possible to implement optically-transparent MOEMS which can be magnetically-actuable by defining specific action regions which are sensitive to external magnetic stimulus.

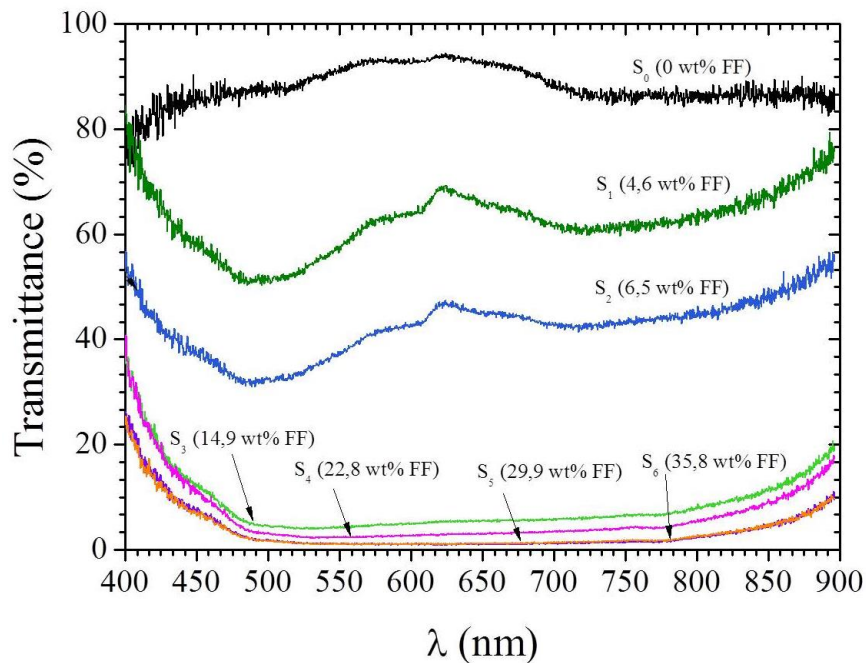


Figure 2.5: Transmittance values in function of wavelength (λ) for magnetic-sensitive stimuli material (M-SSM) samples from S_0 to S_6 which corresponds from 0 wt% FF to 35.8 wt% FF.

2. Results & Discussion

In Table 2.3 the most significant parameters obtained from the M-SSM characterization has been summarized:

2. Results & Discussion

Table 2.3: Summary of the parameters studied in the characterization of M-SSM.

		Sample						
		S ₀	S ₁	S ₂	S ₃	S ₄	S ₅	S ₆
% wt FF		0	4.6	6.5	14.9	22.8	29.9	35.8
Patterning	Curing Time (min.)	20	20	20	20	25	25	30-40
Structural properties	D _{TEM+}	-	-	8 ± 4	-	-	-	7 ± 4
Biocompatibility	Area a ₁	✓	✓	✓	✓	✓	✓	✓
	Area a ₂	✓	✓	✓	✓	✓	✓	✓
	Area a ₃	✓	✓	✓	✓	✓	✓	X
Magnetic properties	m _s (emu/g)	0	0.3 ± 0.2	0.6 ± 0.005	1.5 ± 0.01	2.5 ± 0.005	3.1 ± 0.006	3.6 ± 0.005
	D _L	-	-	6 ± 1	-	-	-	4 ± 1
	D _L	-	-	8 ± 1	-	-	-	6 ± 1
Mechanical properties	Y (kPa)	200	200 ± 100	210 ± 7	400 ± 50	500 ± 300	1000 ± 100	300 ± 200
Optical properties	Mean value T (%)	88.1 ± 0.4	63 ± 3	42.8 ± 0.6	8 ± 3	6.4 ± 0.2	3.5 ± 0.1	3.4 ± 0.8
	Range T (%)	(73-95) ± 1	(50-83) ± 3	(31-57) ± 1	(4-38) ± 3	(2-41) ± 0.5	(0.8-26) ± 1	(0.9-25) ± 2

2. Results & Discussion

2.1.3. *Magnetic-sensitive stimuli material implementation in MOEMS*

From the previously presented results, M-SSM may be a suitable candidate for the development of magnetically actuated MOEMS. However, in order to achieve functional devices, smart designs and fabrication approaches must be developed. In this thesis, two different VOA-MOEMS based on M-SSM (hereafter only mentioned as VOA for simplicity) have been developed. They have an identical design (Figure 2.6), which is composed by a self-alignment element for aligning and clamping of the fiber optics. The waveguide-cantilever has the function of confining the light emerging from the fiber optics. At both sides of such structure two sets of parallel air mirrors [14] have been defined with the aim of having total internal reflection (TIR) conditions at the inner part of the cantilever. A cylindrical microlens has been positioned at the free end of the waveguide-cantilever. Thus, when the light traveling through the waveguide-cantilever reaches the cylindrical microlens the light has been focalized at the collecting fiber optics placed on a second self-alignment. Two reservoirs, which are interconnected via a microchannel which surrounds the waveguide-cantilever has the function of storing either M-SSM (SLT technology) or non-doped PMDS and FF drops (SLT+IJT technology). Using open microfluidics, such polymers will fill the microchannel by capillarity.

Even though the VOAs here presented have the same design, they have been fabricated using two different techniques: in the first case, SLT [15] has been used for defining a VOA with two polymer layers (non-doped PDMS and M-SSM), named as VOA_{SLT} , Figure 2.7. The purpose of the non-doped PDMS layer is to confine the light with low losses due to the high transmittance of the PDMS, whereas the function of the M-SSM layer is to provide the VOA with the capability to be magnetically actuated.

2. Results & Discussion

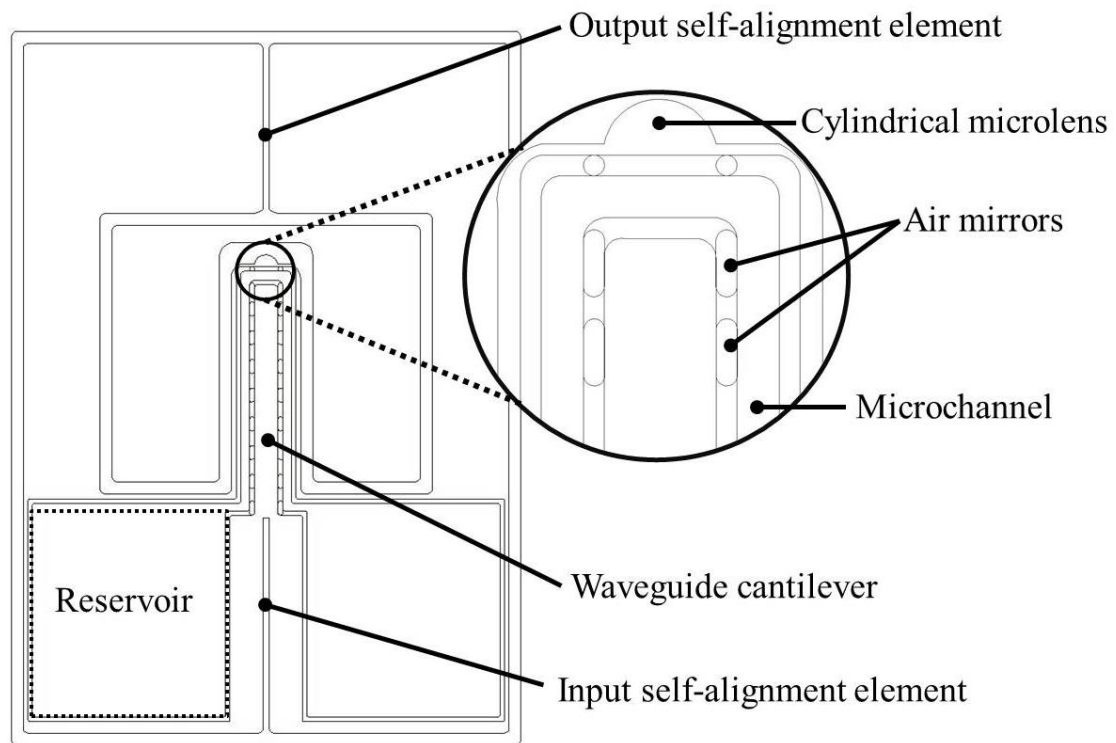
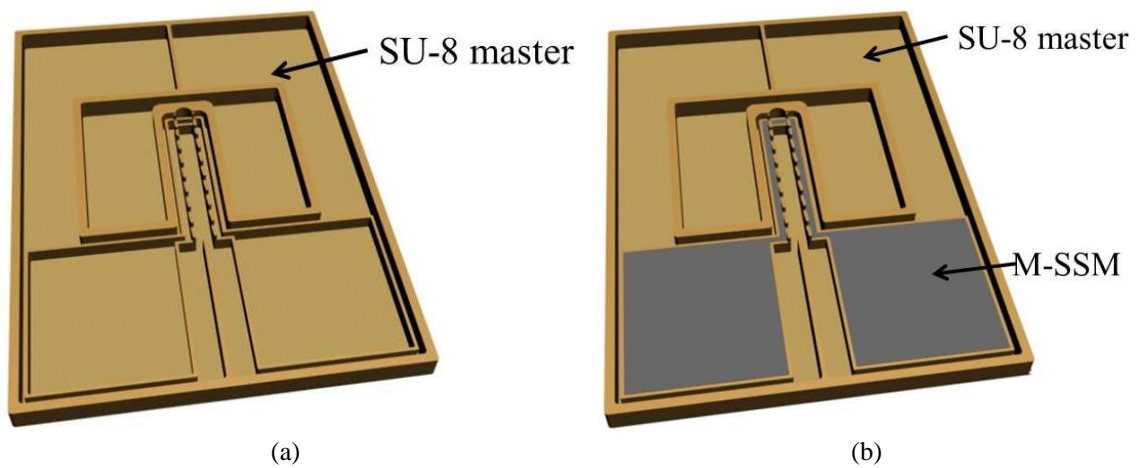


Figure 2.6: VOA design with all the structure in detail: output/input self-alignment element, cylindrical microlens, air mirrors, microchannel, waveguide-cantilever and reservoir.



2. Results & Discussion

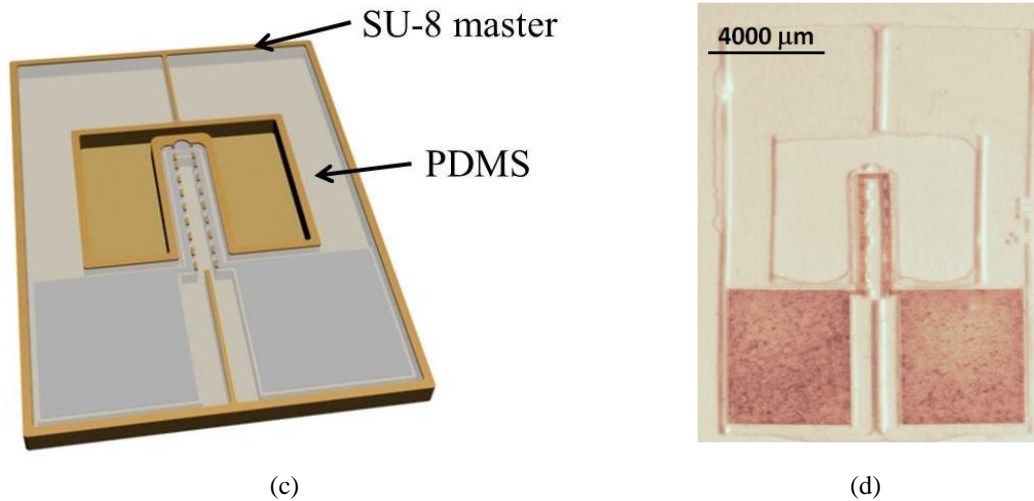


Figure 2.7: Schematic view of the variable optical attenuator fabrication process by soft lithography (VOA_{SLT}): (a) SU-8 master where (b) the M-SSM is placed on the filling regions of the master and (c) the PDMS is also poured on the master. (d) VOA_{SLT} real image after fabrication process.

In order to improve the previous MOEMS (VOA_{SLT}) in the sense of obtaining an enhanced response to the same stimulus, a new system has been fabricated with the same design as previously discussed but implemented with a different approach. In this second case, the IJP technique has been used. In general the IJP or drop delivery technology is an alternative method to pattern liquid samples on a planar substrate. Although resolution is lower than with lithographic methods, this technology requires less volume of fluid to be dispensed on the surface and has larger versatility [16]. It consists on a piezoelectric actuated nozzle, as shown in Figure 2.8. The generation of monodispersed microdroplets, is controlled by the applied voltage on the piezoelectrics, the pulse length and the frequency. Thus, controlled volumes of any liquid (as could be FF) are specifically dispensed at the required positions.

Thus, a second proposed VOA is obtained by combining the SLT with IJP obtaining a VOA_{IJP} . In the first step, non-doped PDMS is poured on the master until it is half filled. While the PDMS is still non-polymerized, IJP technique is used to dispense a given amount of FF droplets ($\sim 165 \cdot \text{pL}$ per droplet) localized at the free end waveguide-cantilever structure and outside of the optical path. Finally, the FF droplets are entrapped with a second, non-doped PDMS, layer resulting in a VOA with the FF entrapped in a clean PDMS matrix, Figure 2.9.

2. Results & Discussion

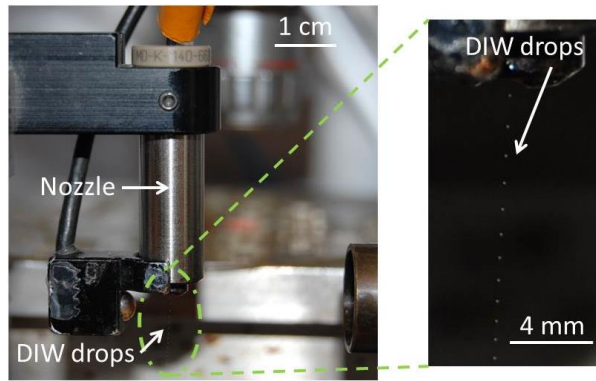


Figure 2.8: A detail of the inkjet printing (IJP) setup for generating deionized water (DIW) microdrops (left image). A real image of the microdrops generation (right image).

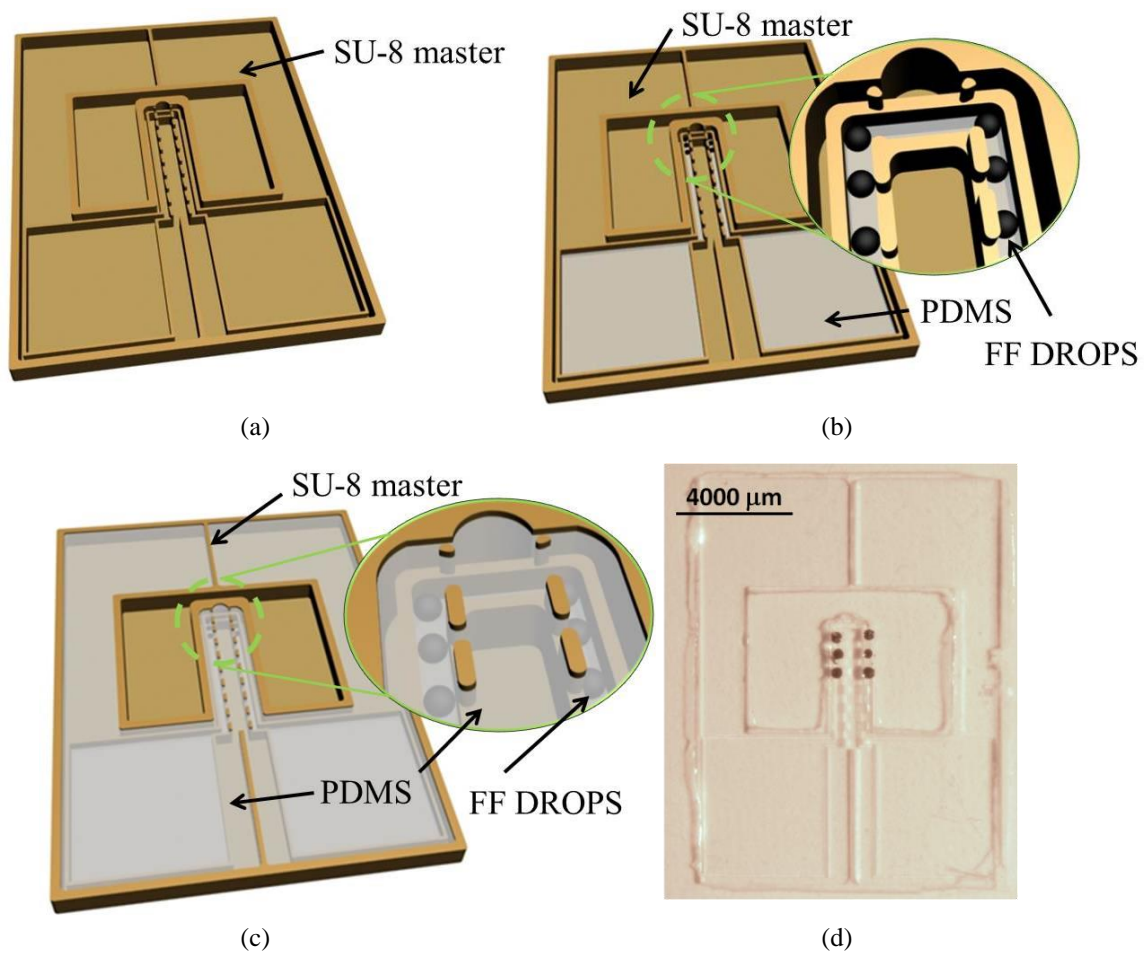


Figure 2.9: Schematic view of the variable optical attenuator fabrication process by IJP (VOA_{IJP}): (a) SU-8 master where (b) the FF drops are placed on the filling regions of the master and (c) the PDMS is also poured on the master covering the FF drops, resulting in drops trapped. (d) VOA_{IJP} real image after fabrication process.

2. Results & Discussion

The VOA_{IJP} presents several advantages as compared to the SLT counterpart: i) mechanically, the FF localization at specific areas assures for the same applied magnetic field (B_{app}), higher deflections at the VOA_{IJP} as compared to the VOA_{SLT} . ii) Optically, the FF has been placed outside the waveguide, so it does not introduce additional light absorption or scattering (see Figure 2.10). Hence, the VOA_{IJP} configuration should result in lower intrinsic losses, (i.e. the losses due to the imperfections of the material or geometries of the device indicating the guiding quality of the optical system) are expectable at the VOA_{IJP} and a higher signal-to-noise ratio (SNR).

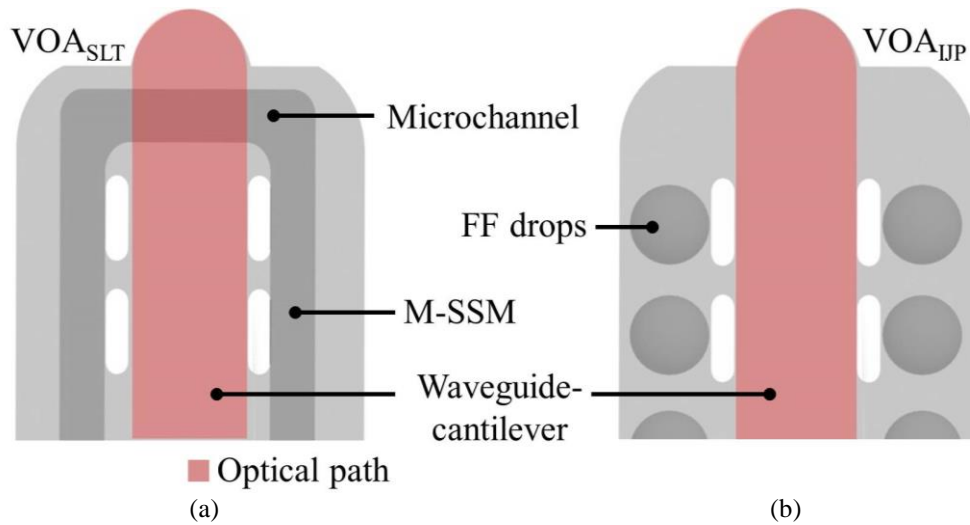


Figure 2.10: (a) and (b) show a detailed schema of both VOAs obtained for SLT and IJP, respectively. The waveguide-cantilever and the optical path are in both cases schematized in red. The U-shaped microchannel where the M-SSM is defined is also shown (left), whereas the position of the FF in the area located in the region where there is no interaction between light and magnetic material avoiding is shown on the right.

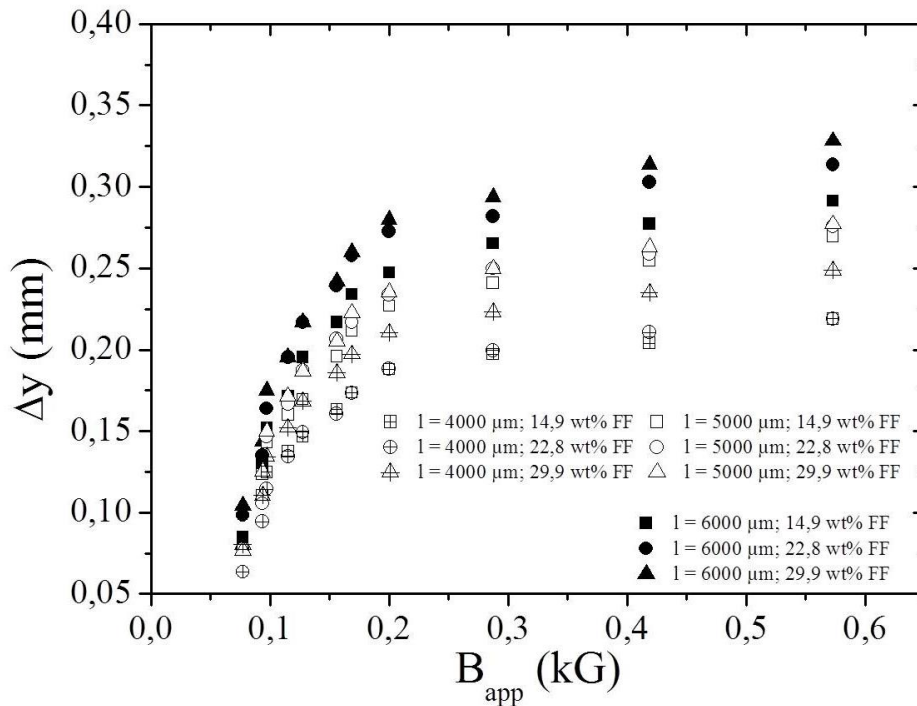
Mechanical characterization

The variation of the deflection (Δy) with the applied magnetic field (B_{app}), for VOA_{SLT} and VOA_{IJP} containing similar FF amount has been studied. Deflections have been measured for all the fabricated VOAs, namely six different FF concentrations (14.9, 22.8 and 29.9 wt% FF in the case of VOA_{SLT} and 14.8, 20.4 and 22.3 wt% FF for VOA_{IJP}). Three waveguide-cantilever lengths ($l_1 = 4000 \mu\text{m}$, $l_2 = 5000 \mu\text{m}$, $l_3 = 6000 \mu\text{m}$) have been used for each fabrication strategy, providing a total of 18 measured VOAs. In both SLT and IJP, deflection increases with B_{app} until a quasi-saturation regime is reached (which has been measured to be between 290-570 G, depending on the specific VOA strategy, length and wt% FF). These results have been presented in Figure 2.11 a) for VOA_{SLT} and 2.11b) for VOA_{IJP} .

2. Results & Discussion

As expected, larger cantilever deflections have been obtained when increasing the wt% of FF in both VOAs. Furthermore, when SLT and IJP technologies are compared, larger deflections have been obtained for VOA_{IJP} containing similar amounts of FF. These results can be associated to the different FF distribution between both strategies: for VOA_{SLT} , the FF is homogeneously dispersed in the M-SSM, which in turn is distributed along the waveguide-cantilever length. For VOA_{IJP} , FF droplets are locally deposited at the free end of the cantilever, making the latter structure more sensitive to B_{app} . Thus, with less loads and a strategic positioning of FF, a higher response at specific B_{app} has been obtained.

Comparing these results with the state of the art it may be concluded that an improvement in the fabrication as well as on the achieved results are obtained. Thus, for low magnetic fields (~ 0.6 kG) and low concentrations of MNP (22.3 wt%) deflections around $0.350 \mu\text{m}$ are obtained. Similar deflections with higher magnetic fields as well as much higher FF concentrations are presented in previously mentioned works (2.95 kG at 70 wt% [17] and 4.1 kG at 40 wt% [2]).



2. Results & Discussion

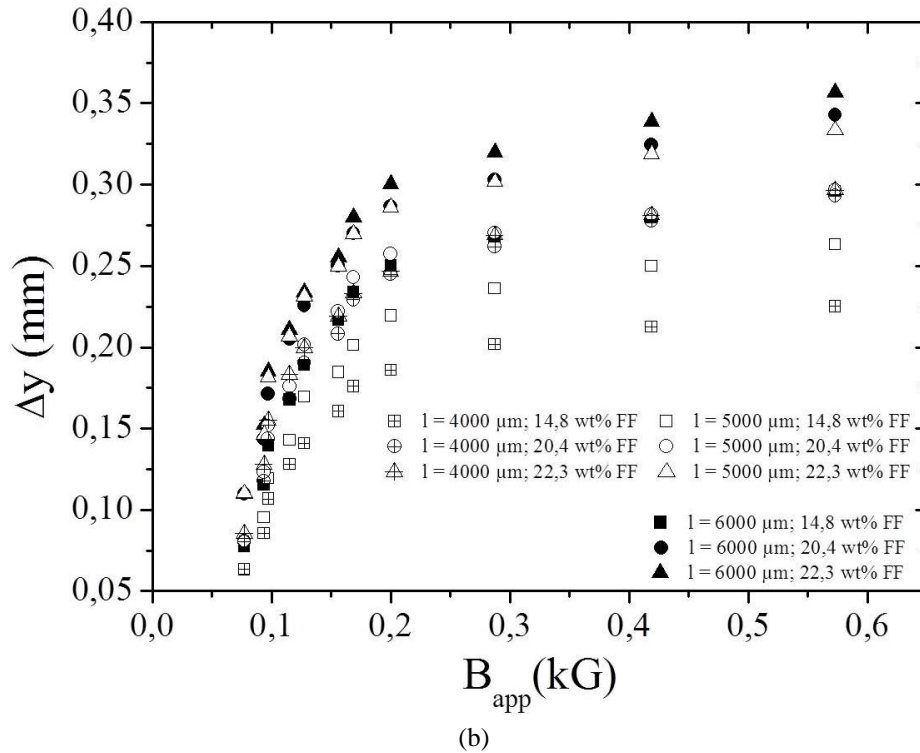


Figure 2.11: Variation of the deflection (Δ_y) in function of the applied magnetic field (B_{app}) for three waveguide lengths (4000 μm , 5000 μm and 6000 μm) for both (a) VOA_{SLT} (concentrations of FF corresponding to 14.9, 22.8 and 29.9 wt% FF) and (b) VOA_{IP} (concentrations of FF corresponding to 14.8, 20.4 and 22.3 wt% FF).

Optical characterization

Optical simulations and experimental results of both VOAs are here presented. Optical intrinsic losses have numerically and experimentally been determined. For both situations the simulation and characterization conditions have been: i) no applied magnetic field ($B_{app} = 0$ kG), ii) a length of waveguide-cantilever of $l_1 = 4000$ μm and iii) the same FF concentrations used in the mechanical characterization.

Numerical simulations have been done using commercial software (Trace Pro, Lambda Research, Littleton, MA, USA). Simulations were performed with a 3D-model of the proposed VOAs. To this effect, light was numerically coupled to the waveguide-cantilever using the specifications of the input and output fiber optics and the previously obtained optical properties for the M-SSM. For accurate simulation of the VOAs, the FF has been also included. Thus, according to the datasheet, the real part of the refractive index (RI) of the FF was $n_{FF}=1.63$ and it is absorbent to all wavelengths in the visible range. The RIs of the M-SSM with different weight fraction of FF were calculated using the Bruggemann effective media approximation [18]. Assuming spherical inclusions of FF in the PDMS (host-material for M-SSM) the RI for each used FF weight fraction has

2. Results & Discussion

been $n_{14,9\%}=1.44$; $n_{22,8\%}=1.46$ and $n_{29,9\%}=1.47$.

From the ray tracing results follows that most of the light is coupled inside the waveguide focusing on the horizontal axis but with different light cross-section profile for VOA_{SLT} (Figure 2.12(a)) and VOA_{IP} (Figure 2.12(b)). The main reason for this distinct behavior is the distribution of magnetic material inside the cantilever in both configurations. The U-shaped microchannel used to define the M-SSM (see Figure 2.10(a)) that orthogonally intersects the optical axis has been designed to be only $50\ \mu\text{m}$ in height, while the total thickness of the VOA is $250\ \mu\text{m}$ (Figure 2.13(a) and (c)). In the VOA_{SLT} this region will have a higher extinction coefficient than the non-doped PDMS, resulting in an increase of the intrinsic losses (Table 2.4). Conversely, in the VOA_{IP} , the microchannel is filled with non-doped PDMS and the FF droplets are placed between the air mirrors and the cantilever lateral facets (outside the optical axis) (see Figure 2.10(b)). Thus, there is no interaction between the confined light and the M-SSM (Figure 2.13(b) and (d)) resulting in a decrease of the intrinsic losses (Table 2.4).

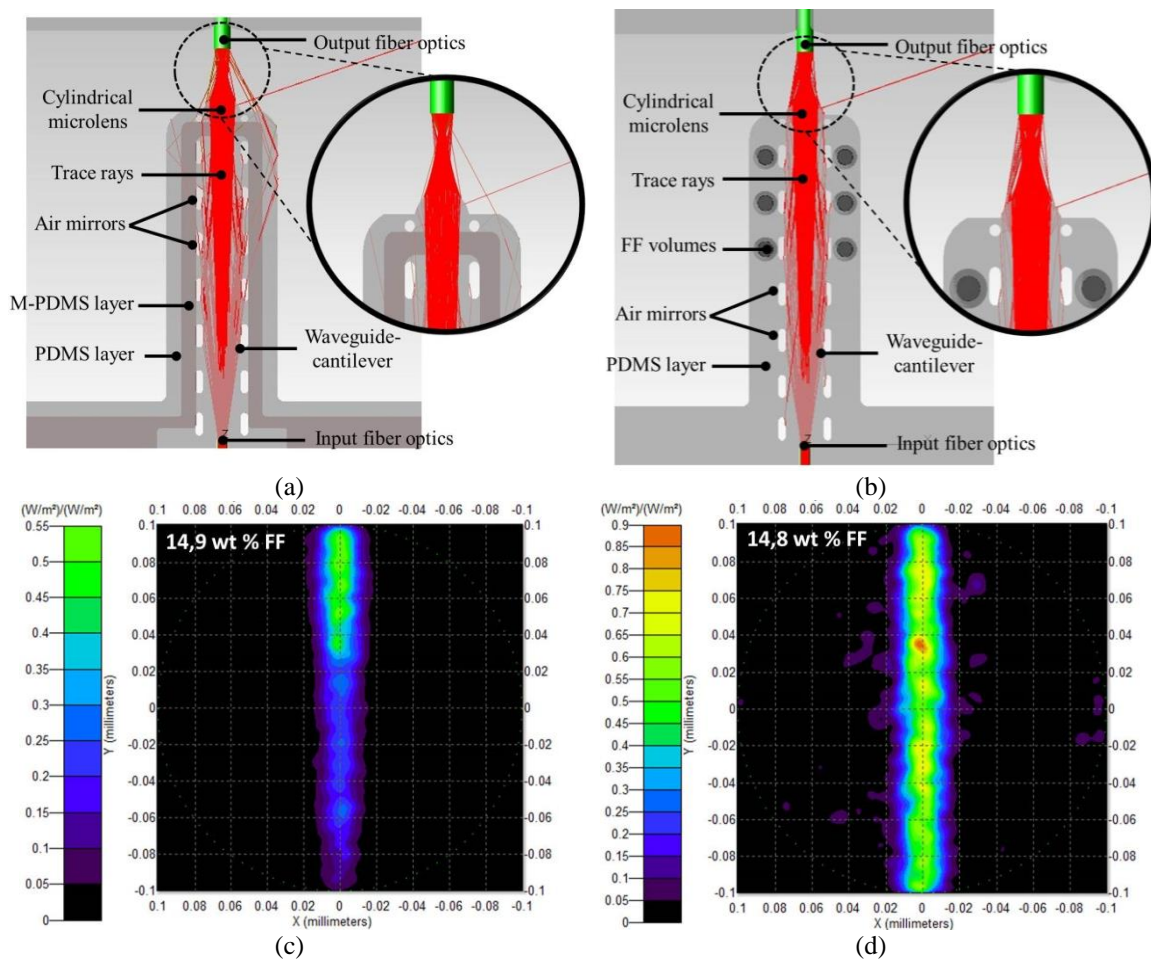


Figure 2.12: Ray-tracing simulation for both VOAs, with $4000\ \mu\text{m}$ length of the waveguide-cantilever and without magnetic actuation ($B_{\text{app}}=0$). Light is guided along the air-mirror-based waveguide and

2. Results & Discussion

focused by the lens for a) VOA_{SLT} (14.9 wt% of FF) and b) VOA_{JIP} (14.8 wt% of FF) at the output fiber optics. Corresponding irradiance maps for c) VOA_{SLT} (14.9 wt% of FF) and d) VOA_{JIP} (14.8 wt% of FF). The cylindrical lens forms in both cases a light sheet, with focusing in the horizontal but not in the vertical axis.

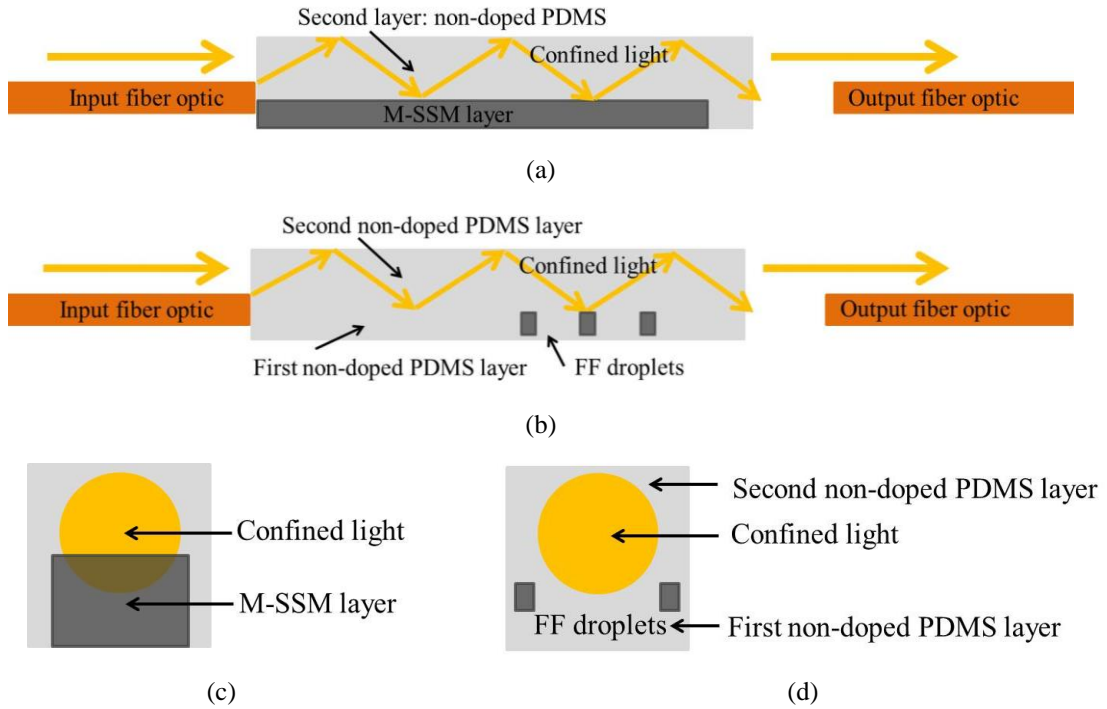


Figure 2.13: Transverse section sketch view of the waveguide-cantilever for (a) VOA_{SLT} and (b) VOA_{JIP} . In both cases the input/output fiber, non-doped PDMS layer, doped PDMS layer, FF droplets distribution and the light path are represented. Moreover, a frontal section sketch view of the waveguide-cantilever where the distribution of the magnetic material and the confined light on the waveguide-cantilever is shown for (c) VOA_{SLT} and (d) VOA_{JIP} .

Table 2.4 summarizes the obtained numerical and experimental intrinsic optical losses. As it can be observed, experimental intrinsic optical losses for VOA_{SLT} increase with the FF concentration, which is in agreement with a higher light absorption/scattering. Conversely, for the VOA_{JIP} , the intrinsic optical losses are independent from FF concentration, since the optical path does not cross the M-SSM.

When comparing these results with previously reported works, it can be seen how Chang-Yen and co-workers obtained intrinsic optical losses close to 17 dB [19]. In our case, in the worst configuration, this magnitude has been measured to be below 10 dB (VOA_{SLT} with 29.9 wt% FF). Thus, the here proposed configuration provides with clear advantages in terms of optical performance.

Table 2.4: Numerically and experimental data for intrinsic optical losses at different wt% FF for VOA_{SLT} and VOA_{JIP} for $l=4000 \mu\text{m}$.

2. Results & Discussion

wt% FF	Intrinsic optical losses VOA _{SLT} (dB)		Intrinsic optical losses VOA _{IJP} (dB)		wt% FF
	VOA _{SLT}	Simulated	Experimental	Simulated	
14.9	7.5	9.0±0.1	4.6	5.1±0.1	14.8
22.8	7.7	9.1±0.2	4.6	5.4±0.1	20.4
29.9	8.0	9.8±0.2	4.6	5.1±0.1	22.3

The difference between the numerical and experimental intrinsic optical losses in both strategies can be associated to fabrication defects, scattering centers at the waveguide cantilever and/or suboptimal positioning of the input/output optical fibers.

Once the intrinsic losses have been determined, actuation losses as a function of B_{app} have been measured. As expected, the higher the FF concentration, the higher the actuation losses. Comparing both technologies, VOA_{IJP} always present higher actuation losses than VOA_{SLT} for a similar FF concentration, (shown in Table 2.5), resulting in a larger dynamic range. Thus, 16.1 dB and 18.9 dB for the VOA_{SLT} and VOA_{IJP}, are respectively obtained. Hence, it can be concluded that with IJP technique, MOEMS with higher actuation losses can be obtained if the FF is located at the cantilever tip.

Table 2.5: Summary of the experimental data obtained from the optical characterization: actuation losses for both VOA_{SLT} and VOA_{IJP} with different FF concentration and for three waveguide lengths.

wt% FF	VOA _{SLT}			VOA _{IJP}			1 (μm)
	14.9	22.8	29.9	14.8	20.4	22.3	
Actuation losses (dB)	10.5	10.9	12.1	12.1	13.7	16.3	4000
	11.5	12.1	12.5	13.1	14.3	16.8	5000
	12.6	13.8	16.1	14.8	15.4	18.9	6000

2.2. Light-sensitive stimuli material

This second section focuses on light-sensitive stimuli material (L-SSM) based on two different negative-tone photoresists (Epocore and SU-8) as matrix materials and non-polar dyes as dopant to obtain the L-SSM_{Epo} and L-SSM_{SU-8}, respectively. Similar to the M-SSM, the polymerization of the doped resist has been tested as function of the dye concentration. Optical properties of both L-SSMs have been obtained by defining test structures with specific dye concentration and different optical paths. This has allowed knowing which optical paths and dye concentrations are optimal for their further implementation in optically-actuated variable optical attenuator (VOA) components. The main idea in this section is to develop a microsystem where both L-SSM and non-doped photoresist are combined. The non-doped version has been used to

2. Results & Discussion

define the mechanical structures and the optical waveguides in the MOEMS, while the doped version has been used exclusively to define the actuation points. In this case, the actuation has been achieved by focusing light with the appropriated wavelength. Thus, resulting in a thermal expansion of the L-SSM is accomplished, inducing the required movement and, in general, actuation over the MOEMS.

2.2.1. Light-sensitive stimuli material synthesis

Two different photoresists have been used for defining the L-SSM. In the first case (L-SSM_{Epo}) 25 mg of the Epocore photoresist has been mixed with 1 mg of non-polar dyes (Proquimac Color, Spain) with three different spectral responses (lilac, red and yellow) with a ratio of 25:1. For the second material, 25 mg of SU-8 2005 photoresist has been mixed with 50 mg of color dye (yellow, orange, red, lilac, blue, green) obtaining the L-SSM_{SU-8} with a ratio of 25:2.

2.2.2. Light-sensitive stimuli material Epocore based: photopatternable study test structures

Photopatternable study

The first experiment that has been performed is to determine how the inclusion of dopants in the photoresist modifies its photopatternable properties. To this effect, the dye-doped Epocore has been obtained by mixing 1mg for each dye per 25 g of Epocore (1:2500 ratio). Here a dye-doped Epocore 50 μm -thick layer has been spun (1500 rpm for 60 s) on a pre-cleaned glass substrate. After the required soft-bake (SB) (5 min at 50 $^{\circ}\text{C}$, bake 7 min at 90 $^{\circ}\text{C}$), the different substrates have been exposed to four different doses (from 500 mJ/cm^2 to 2500 mJ/cm^2) of UV-light at 365 nm using the appropriate mask. It has been followed by the post-exposure bake (PEB) (5 min at 50 $^{\circ}\text{C}$ ramp up to 85 $^{\circ}\text{C}$, bake 10 mi at 85 $^{\circ}\text{C}$ and slowly cool down). Finally, the development step where the structures have been immersed during 180 s in PGMEA has been carried out, where the unexposed photresist has been removed. The resulting structures (Insets in Figure 2.14) consisting on arrays of lines with widths and distances between consecutive lines ranging from 1 μm to 100 μm , are presented in Figure 2.14. As it can be seen, all L-SSM_{Epo} structures (using the three dyes under study) are crack-free. Moreover, the structurability of the L-SSM_{Epo} in such test structures is maintained with a reduction on

2. Results & Discussion

the resolution when compared to the non-doped case, as expected. For the highest tested dose, although T-topping effect can be clearly seen in Lilac doped L-SSM_{Epo}, no dye leaching is observed. Thus, it can be concluded that the L-SSM_{Epo} polymerization process is stable for the three dyes under study, and it is possible to fabricate structures with a minimum resolution of 7 μm .

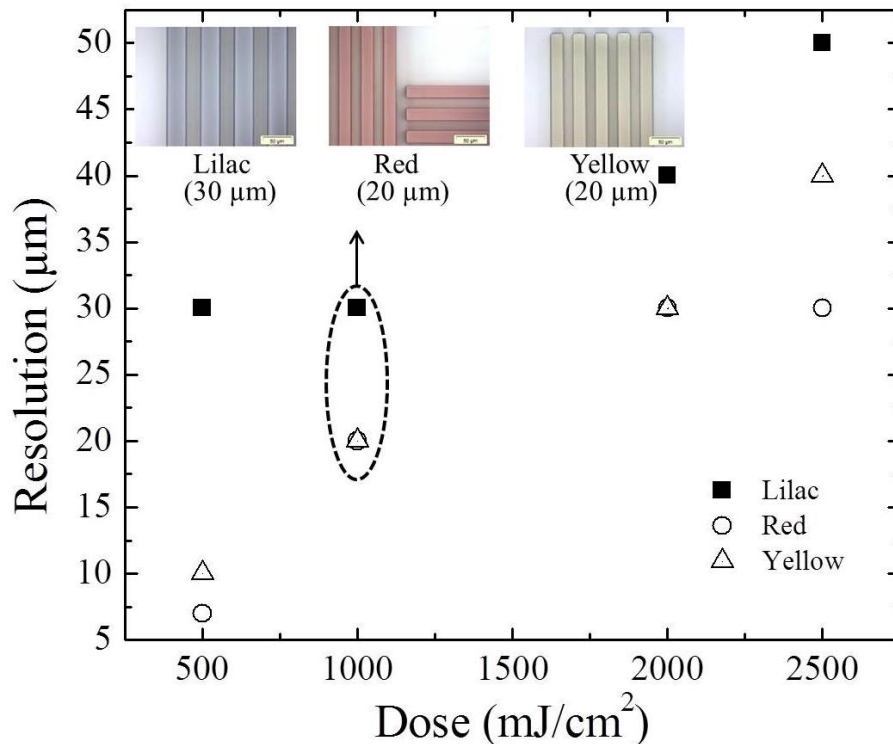


Figure 2.14: Images from the photolithographic process of the lilac-, red- and yellow-doped L-SSM_{Epo} for different doses.

2.2.3. Light-sensitive stimuli material Epocore and SU-8 based test structures

Design

Optical test structures have been designed with the purpose of studying the spectral response of the L-SSM as a function of both the optical path and the dye color concentration. Such structures consist on a microfluidic channel with a single inlet/outlet and different sections with an increasing width ranging from 100 μm up to 3000 μm , as can be seen in Figure 2.15. When filled with either dye-doped L-SSM_{Epo} or L-SSM_{SU-8}, the structure can be envisaged as an absorbance filter from which, it

2. Results & Discussion

becomes possible to determine the spectral response of both L-SSM. Two self-alignment elements have been placed at each side of the filter to assure the accurate positioning of in- and out-put optical fibers used to inject and collect the light and analyze the optical response of the developed materials. A microlens has been placed at the end of each self-alignment microchannel [20] to correct the beam broadening due to the fiber numerical aperture.

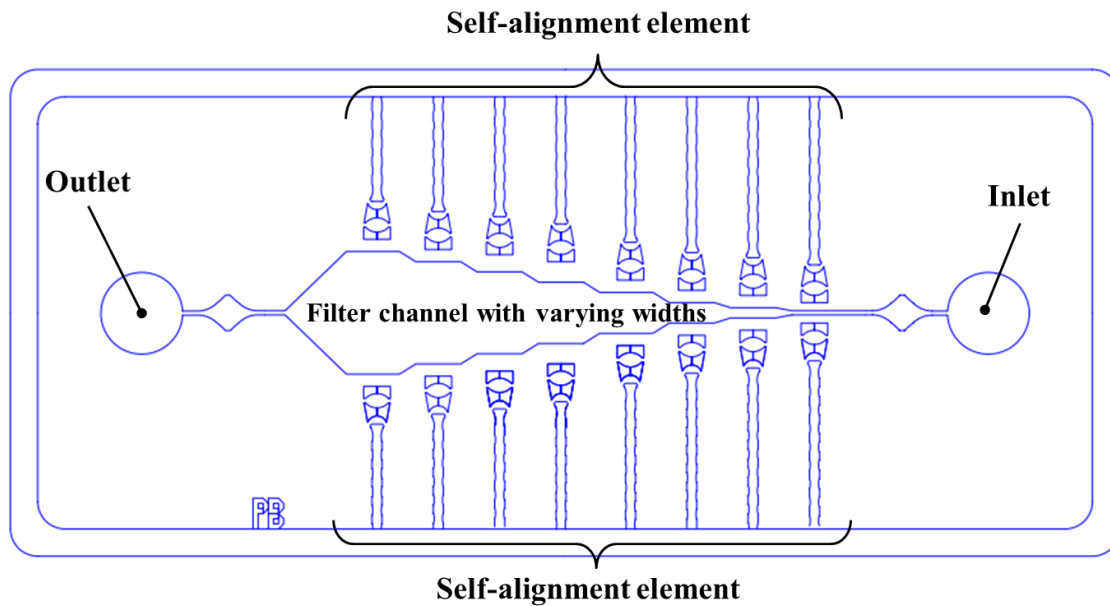


Figure 2.15: Design of the optical test structure composed of self-alignment microchannels for positioning of input/output optical fibers and a continuous microfluidic channel with varying widths

Fabrication

The fabrication of the optical test structures is identical for both L-SSMs. It starts with the implementation of an SU-8 2050 (MicroChem, Corp., Newton, MA, USA) master [21]. In parallel, PDMS is prepared by mixing the curing agent and the elastomer in a proportion 1:10 (v:v). The resulting mixture is poured over the SU-8 master. After the curing process the polymerized PDMS is peeled off from the master. To finalize the process, the patterned PDMS samples are bonded to an activated glass substrate by oxygen plasma (PVA TePla AG, Munich, Germany). Parameters of bonding are: 12 s for exposition time; 200 W of power and 90 mbar corresponding to the pressure. After that, the obtained L-SSMs (section 2.2.1.) are dispensed at the inlet and by capillary forces the structure is completely filled. Then, UV light (365 nm, 300 mJ/cm²) is used to generate the photo-acid on both materials. Finally, a PEB allows the polymerization of the optical test structures, as shown in Figure 2.16.

2. Results & Discussion

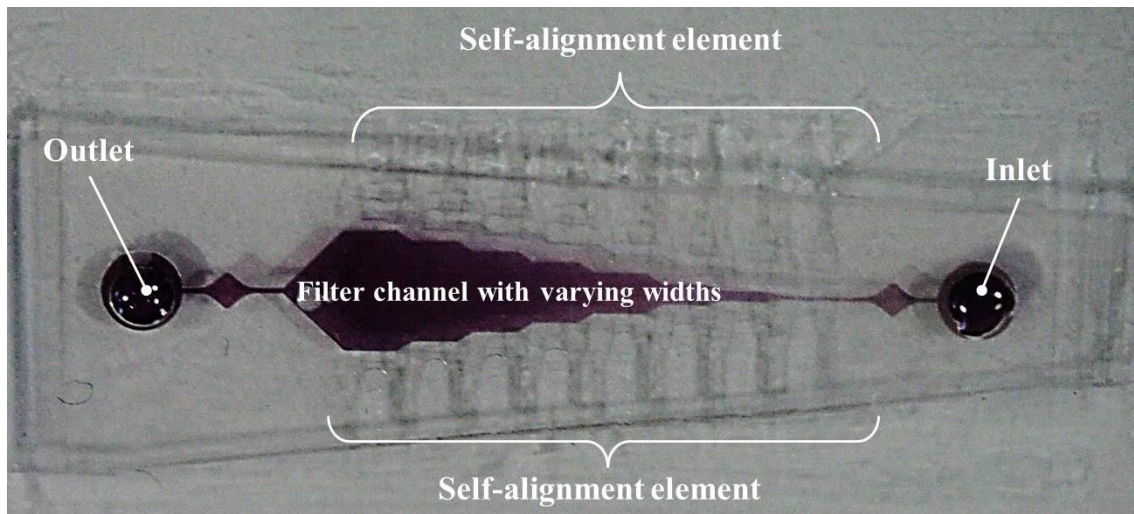


Figure 2.16: Real image of the optical test structure composed of self-alignment microchannels for positioning of input/output optical fibers and a continuous microfluidic channel with varying widths

Optical characterization

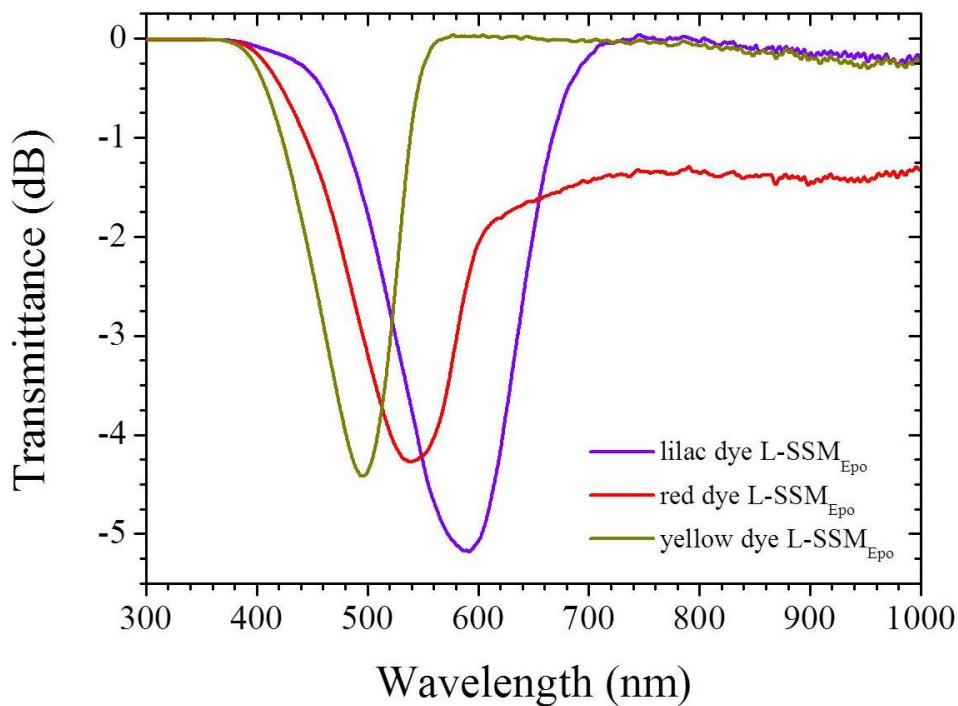
Optical test structures have been used to determine the spectral response of both the L-SSM_{Ep0} and L-SSM_{SU-8} using different colored dyes. To this end, a white light lamp (HL-2000 FHSA, Ocean Optics, Germany) coupled to an optical fiber (230 μm diameter, Thorlabs, Dachau/Munich, Germany), has been used as light source. The light outcoming from the optical test structure has been collected by an identical fiber optics (located at the second self-alignment element) and connected to a microspectrometer (USB2000+ Ocean Optics, Dunedin, FL, USA).

The obtained optical test structures present different stopbands (region where absorption at specific wavelengths is observed) depending on the dye used for implementing the L-SSM: 5.17 dB@592nm, 3.30 dB@531nm, 4.40 dB@497 nm, for lilac-, red- and yellow L-SSM_{Ep0}, respectively. Regarding the passband (region where a high transmittance at specific wavelengths is observed): yellow and lilac have the optimal zero passband penalty as discussed above, whereas red-L-SSM_{Ep0} has a small, but non-zero passband for wavelengths above 700 nm (0.75 dB), Figure 2.17(a). For the case of L-SSM_{SU-8} the same optical study has been carried out, see Figure 2.17(b). Here, L-SSM_{SU-8} presents stopbands of: 5.9 dB@502 nm; 7.8 dB@530 nm; 10.1 dB@582 nm; 11.69 dB@657 nm and 12.0 dB @653 nm for yellow, orange, red, green and lilac, respectively. Although the concentration for L-MSS_{SU-8} is higher, all of them present an

2. Results & Discussion

optimal zero passband, higher attenuation for the maximum stopband and a broader bandwidth when compared to $L\text{-MSS}_{\text{Epo}}$.

From these results, it can be concluded that the characterized L-MSS's based on photopatternable resists present the theoretical behavior which is expectable in absorbance filters, and the results obtained can be compared with these previously published [22]. Other thermocurable materials such as doped PDMS [23] or even more technologically complex, such as highly porous nanostructured metal-oxide film with a monolayer of dye molecules present in both cases non-zero passband penalty [24]. In addition, the dye color allow to define UV-patternable band-rejection filters (allowing to block specific wavelengths), as opposite to the more common cases in absorbance filters, where either high-passband or low-passband filters are obtained. When combining these two aspects, it can be foreseen that the optical testing elements can indeed be used for the implementation of light actuated devices [25].



(a)

2. Results & Discussion

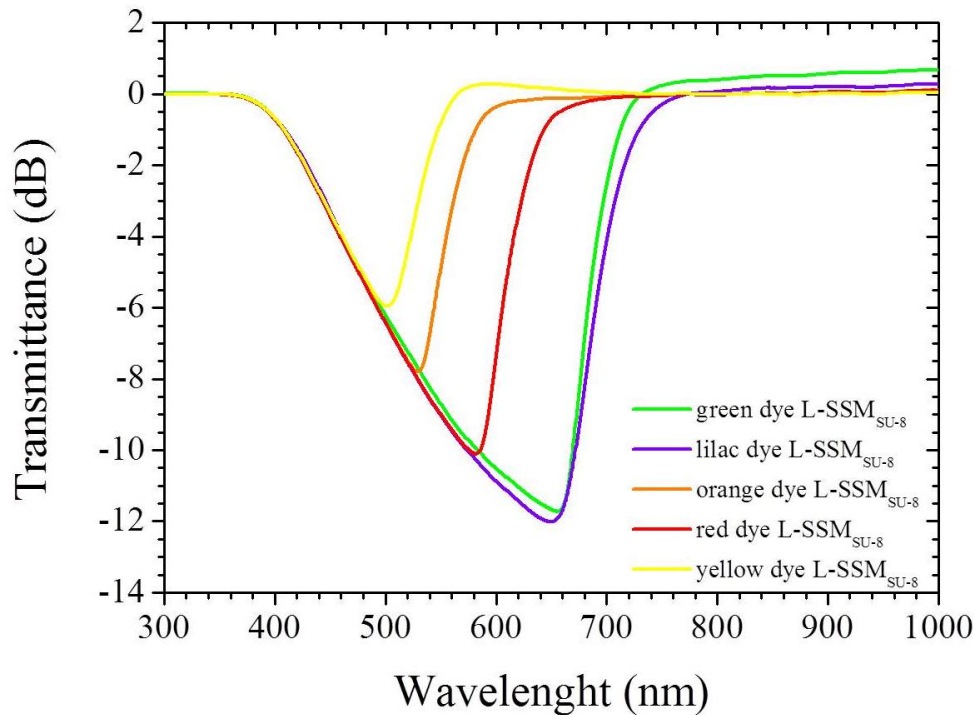


Figure 2.17: Spectral response for (a) lilac, red and yellow L-SSM_{Epo} (Epocore 25:1 dye) and for (b) green, lilac, orange, red and yellow L-SSM_{SU-8} (SU-8 25:2 dye).

Red light-sensitive stimuli SU-8 based

As mention in the last section, both L-SSM_{Epo} and L-SSM_{SU-8} could be interesting for *applications where wavelength filtering is required, such as for the implementation of light actuated devices*. So, at this point, the choice of one of these materials has to be elected for its application in a system. This has been based on which one has a higher transmittance value and which is possible to measure according to the tools present in the laboratory (i.e. basically lasers). Thus, if two materials have been compared, according to their transmittance values it has been concluded that the L-SSM_{SU-8} (5.9 dB@502 nm; 7.8 dB@530 nm; 10.1 dB@582 nm; 11.69 dB@657 nm and 12.0 dB @653 nm for yellow, orange, red, green and lilac, respectively) has higher values than the L-SSM_{Epo} (5.17 dB@592nm, 3.30 dB@531nm, 4.40 dB@497 nm, for lilac-, red- and yellow, respectively). From these values and according to the available tools in the laboratory the yellow L-SSM_{SU-8} and the red L-SSM_{SU-8} are the two potential candidates with which it could be work. Red L-SSM_{SU-8} have a higher transmittance (10.1 dB@582 nm) compared to the yellow L-SSM_{SU-8} (5.9 dB@502 nm). Thus, the red L-SSM_{SU-8} will be chosen to apply an actuated device. Therefore optical and thermal characterization of this red L-SSM_{SU-8} presented below, followed by

2. Results & Discussion

its implementation in a micro-opto-electro-mechanical system variable optical attenuator (VOA-MOEMS).

Optical characterization

The absorbance of a 50 mg of red dye-doped SU-8 filter for six different path lengths (100 μm , 250 μm , 500 μm , 1000 μm , 1500 μm and 2000 μm) has been characterized. For its validation a fiber-optic is connectorized to a halogen lamp (HL-2000 FHSA, Ocean Optics, Germany), and a microspectrometer (USB2000+, Ocean Optics, Germany). Results on Figure 2.18 show a growing tendency as a function of the path length until a saturate value close to 1500 μm has been reached. For this path length which corresponds to the dimensions of the actuation element designed on the VOA-MOEMS (see *Red light sensitive stimuli SU-8 based implemented on a VOA-MOEMSs (Design) section*) with an absorbance of 10.08 dB has been chosen for its implementation on such actuated systems.

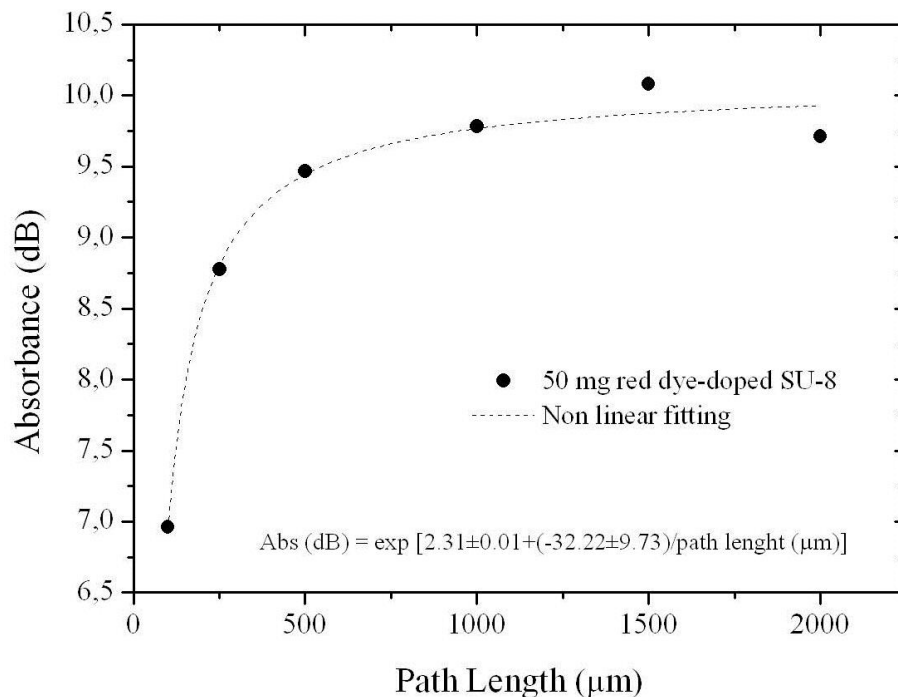


Figure 2.18: Absorbance experimental results in function of different path length corresponding to a 50 mg red dye-doped SU-8 filter.

2. Results & Discussion

Thermal Properties

SU-8 has a coefficient of thermal expansion of 52 ppm. This coefficient expresses a change in the size of a material in response to a change in the temperature on the material. With the intention of verifying which is the increase in temperature of the L-SSM_{SU-8} a thermal characterization has been carried out. The experiment consists on infrared (IR) camera measurements of the radiance on the L-SSM_{SU-8} with and without an external actuation. The corresponding camera software gives the temperature data (T). Specifically, the geometry of the L-SSM_{SU-8} sample corresponds to 1500 μm of diameter area where a light beam with the appropriate wavelength is directed.

Initially T has been measured without external actuation obtaining a $T \sim 29^\circ$. By applying the actuation from a green diode laser (Laser Nano, 532 nm, 105 mW, Qioptiq, Germany), the temperature (T') has been measured again. Thus, the variation of temperature corresponds to $\Delta T = T' - T$. But having $T \sim 29^\circ \text{C}$ which is close to the room temperature, ΔT can be considered as the T'. Thus, temperatures have been measured turning on the laser and focusing it on the L-SSM_{SU-8} sample and then turning it off. Thus ΔT_2 is higher than ΔT_1 and ΔT_3 higher than ΔT_1 and ΔT_2 . But ΔT_4 is the lowest value comparing with the other temperatures. This must be due to a material degradation after several laser focusing on the L-SSM_{SU-8}

$$\Delta T_1 = 84^\circ\text{C}; \Delta T_2 = 114^\circ\text{C}; \Delta T_3 = 105^\circ\text{C}; \Delta T_4 = 73^\circ\text{C}$$

$$\langle \Delta T \rangle = 94^\circ\text{C}$$

$$\sigma_{\Delta T} = 32$$

$$\Delta T = (94 \pm 32)^\circ\text{C}$$

2.2.4. Red light sensitive stimuli SU-8based implemented on a VOA-MOEMSs

Design

Opto-mechanically, the proposed VOA-MOEMS is the logical evolution from a previous work developed at IMB-CNM, CSIC (Spain) in collaboration with the Institut für Mikrotechnik (Braunschweig) [26]. Mechanically, it consists of four mechanical beams that clamp the seismic mass to the frame, preventing angular misalignment. Optically, three waveguides are defined at the mechanical structure, whereas fish-bone elements align and clamp the input and output fiber optics in the same optical axis as

2. Results & Discussion

the waveguide. When actuation is OFF state, the fiber optics and the waveguide are aligned and thus the actuation losses (losses due to the working principles of the structure) have a zero value. When actuation is ON, the mass displacements result in a misalignment between the waveguide and the input/output fiber optics (Figure 2.19). Thus, in the proposed VOA-MOEMS, the actuation losses are modulated as a function of the actuation principle.

Actuation is achieved by defining four actuation points on each VOA-MOEMS which are anchored at the mechanical beams close to the frame. These actuation points consist on structured L-SSM_{SU-8}. Absorbed light causes localized heating and expansion of dye-doped polymer. This change in volume is transferred to the polymer mechanical beams, resulting in an overall displacement of the quad beam structure as a function of the focused light intensity.

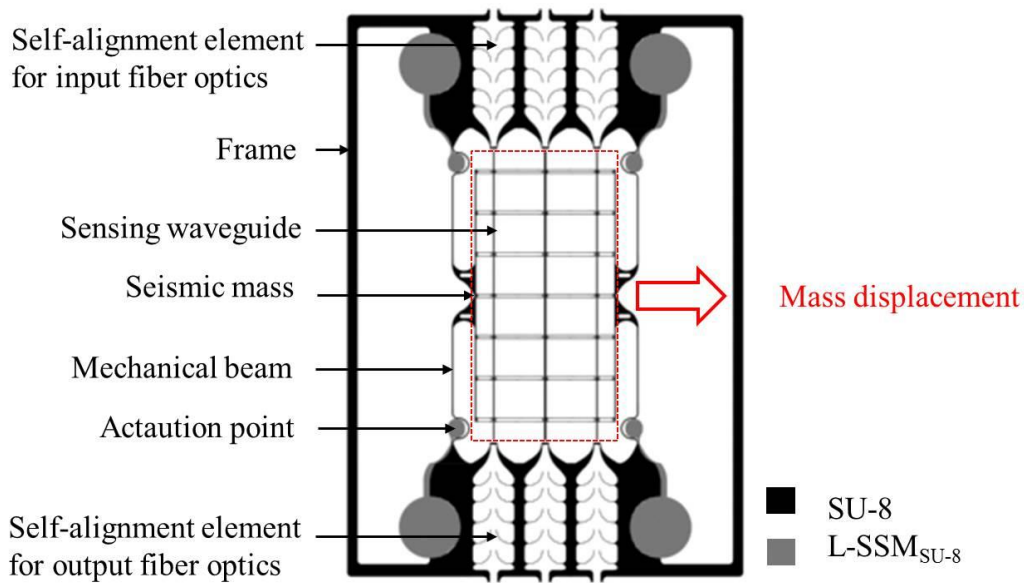


Figure 2.19: Top view scheme of the polymeric VOA-MOEMS comprising a quad beam mechanical structure, waveguides, self-alignment elements and L-SSM_{SU-8}-based actuation points.

Optical simulations

The proposed working principle (modulation of the losses as a function of the misalignment) was numerically verified. Optical simulations of the proposed VOA-MOEMS have been performed using the TracePro software (Lambda Research, Littleton, MA, USA). It consists on a 3D-model mimicking the real VOA-MOEMS. Figure 2.20 (a), (b) and (c) shows ray tracing results (red lines) along the waveguide-cantilever into the SU-8 waveguides in the case of no lateral misalignment between the waveguide-

2. Results & Discussion

cantilever and the output optical fiber ($\Delta x = 0 \mu\text{m}$), i. e. no optical actuation, and $\Delta x = 12 \mu\text{m}$ and $\Delta x = 25 \mu\text{m}$, respectively. Moreover, irradiance maps in Figure 2.20 (d), (e) and (f) corresponding to the increasing Δx s, are included showing a dramatic decrease of the rays reaching the output fibers as Δx increases.

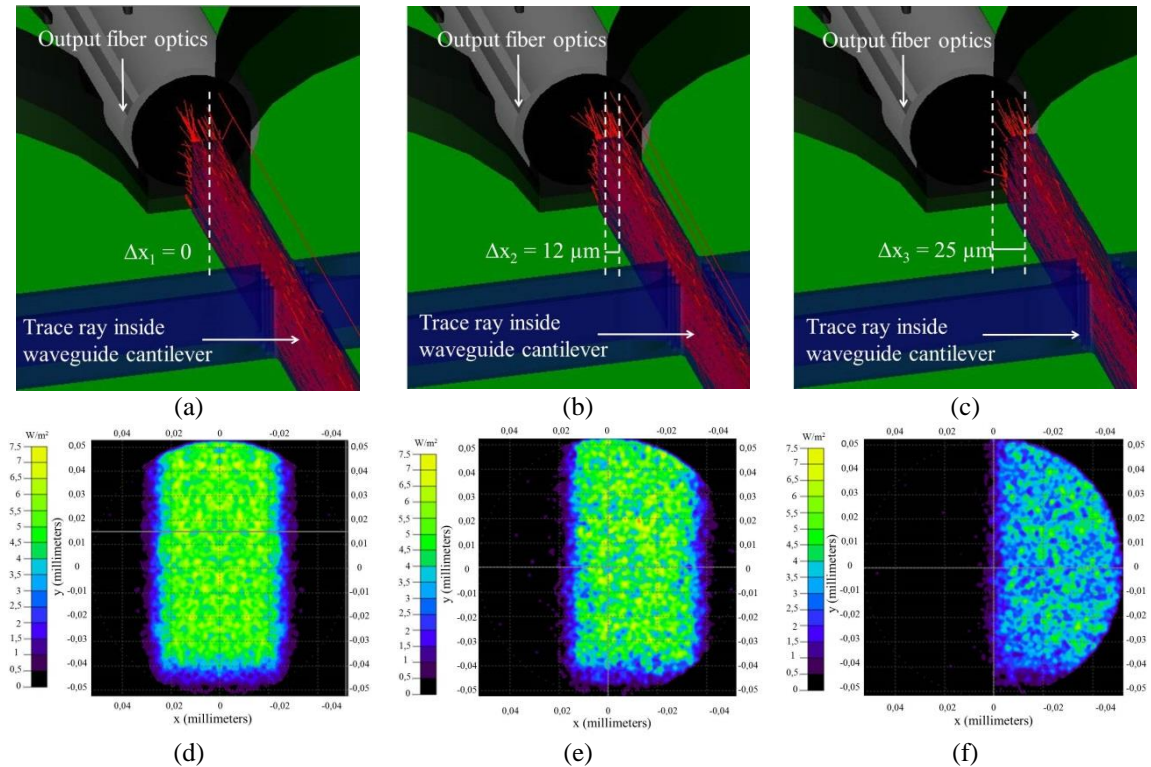


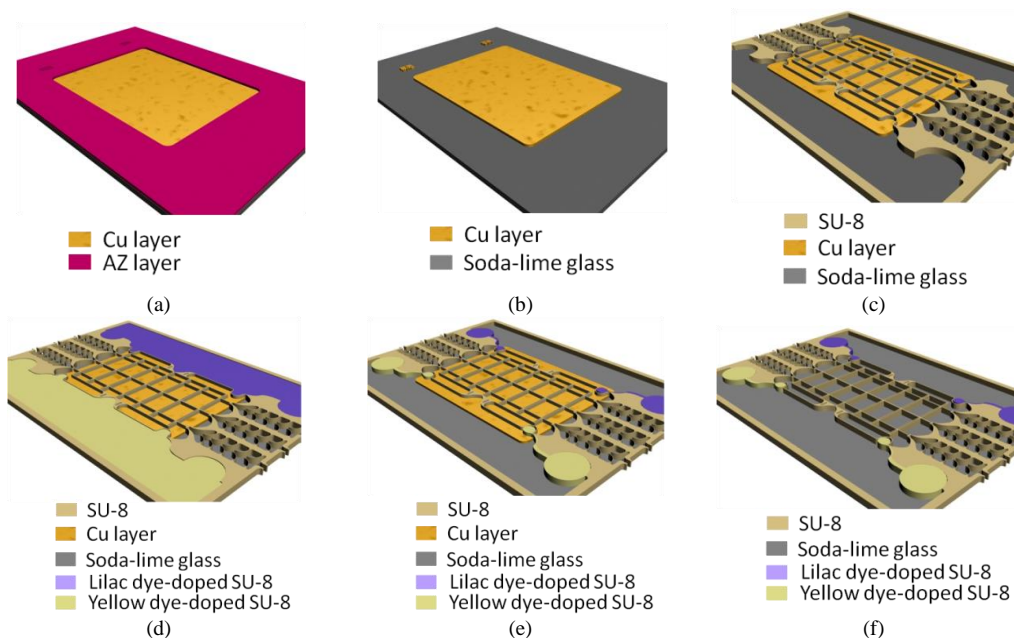
Figure 2.20: (a), (b) and (c), ray tracing simulation for VOA-MOEMS. and (d), (e) and (f) corresponding irradiance maps showing the light profile cross the section at the output for $\Delta x = 0 \mu\text{m}$, $\Delta x = 12 \mu\text{m}$ and $\Delta x = 25 \mu\text{m}$, respectively. .

Fabrication

The fabrication process starts on a $700 \mu\text{m}$ thick soda-lime glass, which is used as a substrate. 20 nm Cr layer and 200 nm Cu seed layer are evaporated on the substrate. Then, a photoresist (AZ9260, MicroChemicals GmbH, Ulm, Germany) is spun obtaining a thickness of $25 \mu\text{m}$. After that, a first photolithographic mask defines the regions where the Cu seed layer will be electroplated obtaining a $20 \mu\text{m}$ -thick Cu layer, Figure 2.21(a), following by rinsing in acetone to remove the photoresist. A short dip in Cu etch removes the Cu seed layer, Figure 2.21(b). Then, a layer of SU-8 is spun (SU-8 2050, MicroChem Corporation, Newton, MA) obtaining a thickness of $125 \mu\text{m}$. After a relaxation time of 20 minutes, wafers are soft baked (SB) for 2h at $95 \text{ }^\circ\text{C}$ on a hotplate. Then, the wafer is exposed to UV light (365 nm , 350 mJ/cm^2) using a second photolithographic mask required for defining the optomechanical parts of the VOA-

2. Results & Discussion

MOEMS (self-alignment system for input/output fiber optics, sensing waveguide, mechanical beams, seismic mass and the frame) followed by a post exposure bake (PEB) for 20 minutes at 95 °C. The first development step is then carried out by immersing the wafers in propylene glycol methyl ether acetate (PGMEA, MicroChem Corporation, Newton, MA), Figure 2.21(c). For further mechanical stabilization and cross-linking enhancement a hard bake (HB) for 2 h at 120 °C under nitrogen atmosphere is done. At this point the L-SSM_{SU-8} dye-doped is poured on the regions that have been defined between the frame and the mechanical beam, Figure 2.21(d), with a relaxation time of 20 minutes and a SB for 2h at 95 °C on a hotplate. Specifically, in this work the red dye has been mixed with the SU-8 in 25:2 ratio. Here a second exposition to UV light (365 nm, 2.5J/cm²) is required by using a third photolithographic mask for defining the optical actuation elements followed by a PEB for 20 minutes at 95 °C. A second development step followed by a HB for 2 h at 120 °C under nitrogen atmosphere is done, Figure 2.21(e), too. The final part consists of an etching of the sacrificial layer, Figure 2.21(f). At this point, the VOA MOEMS structures are released, Figure 2.21(g), finishes the fabrication process.



2. Results & Discussion

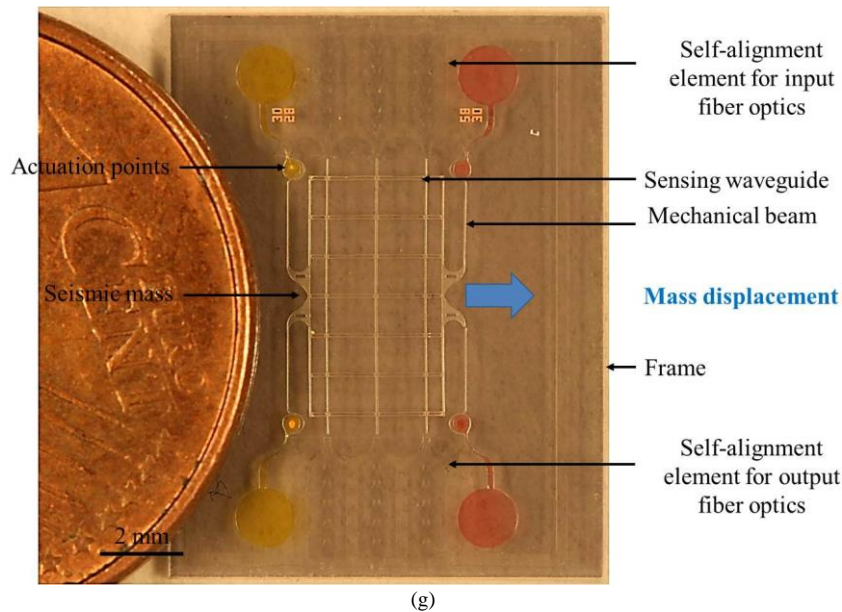


Figure 2.21: Scheme of the fabrication process starting with (a) AZ9260 photoresist and the first mask the area to obtain a 20 μm -thick Cu electroplating layer is defined. (b) After that the photoresist is removed by acetone. Here, (c) 125 μm of SU-8 is spun on the wafer where after using the second mask and the corresponding development the optomechanical parts of the VOA (self-alignment system for input/output fiber optics, sensing waveguide, mechanical beams, seismic mass and the frame) are defined. (d) The red-dye doped SU-8 is poured on the regions that have been defined between the frame and the mechanical beam. (e) Then, after using a third mask and the development of the doped SU-8 the definition of the actuation points are achieved. Finally, (f) after an etching of the sacrificial layer the VOA-MOEMS is completely finished. (g) Image of the completely fabricated VOA with the mechanical and the actuation points.

Optical characterization of red light-sensitive stimuli implemented into VOA-MOEMS

Final validation of the proposed VOA-MOEMS requires two different light sources, as it can be seen in Figure 2.22(a): the actuation is done by directing a green diode laser (Laser Nano, 532 nm, 105 mW, Qioptiq, Germany) at the actuation point. The focus had a spot diameter of 670 μm , resulting in an applied power of 7.7 W/cm^2 at maximum actuation efficiency. The wavelength of this laser presents the highest absorption for the red doped L-SSM_{SU-8} according to the values obtained in the section 2.2.4. An additional 635 nm diode laser (Laser source, 635 nm, 2.5 mW, Model S1FC, Thorlabs GmbH, USA) is coupled at the input fiber optics of the VOA-MOEMS and is used as sensing wavelength. Light variations in the sensing wavelength due to actuation are measured using an optic fiber connected to a microspectrometer (USB2000+, Ocean Optics, Germany) which collects the output light arising from the waveguide (Figure 2.22(b)).

2. Results & Discussion

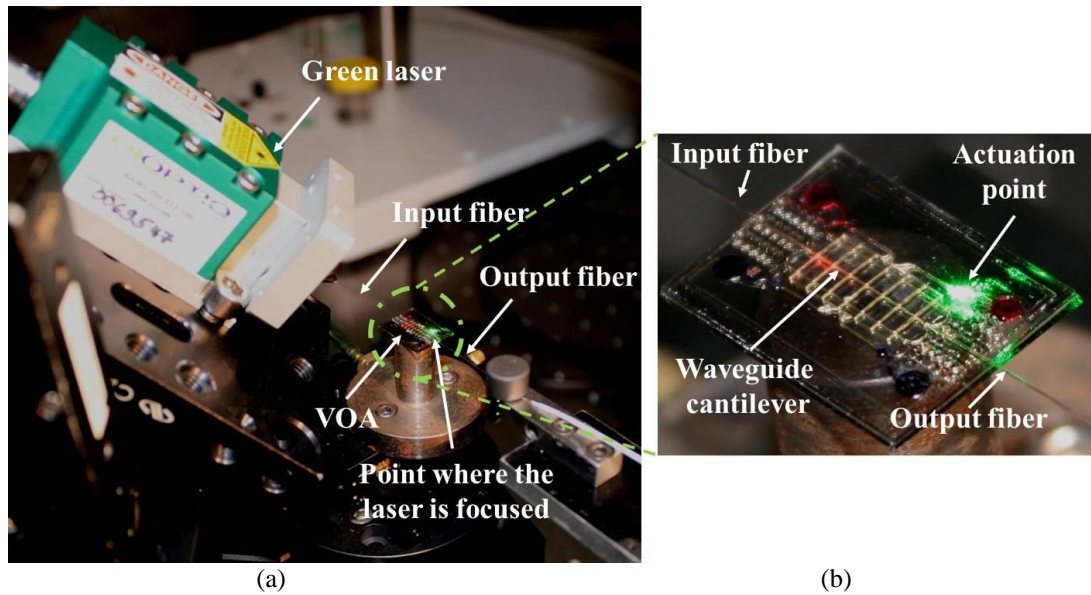
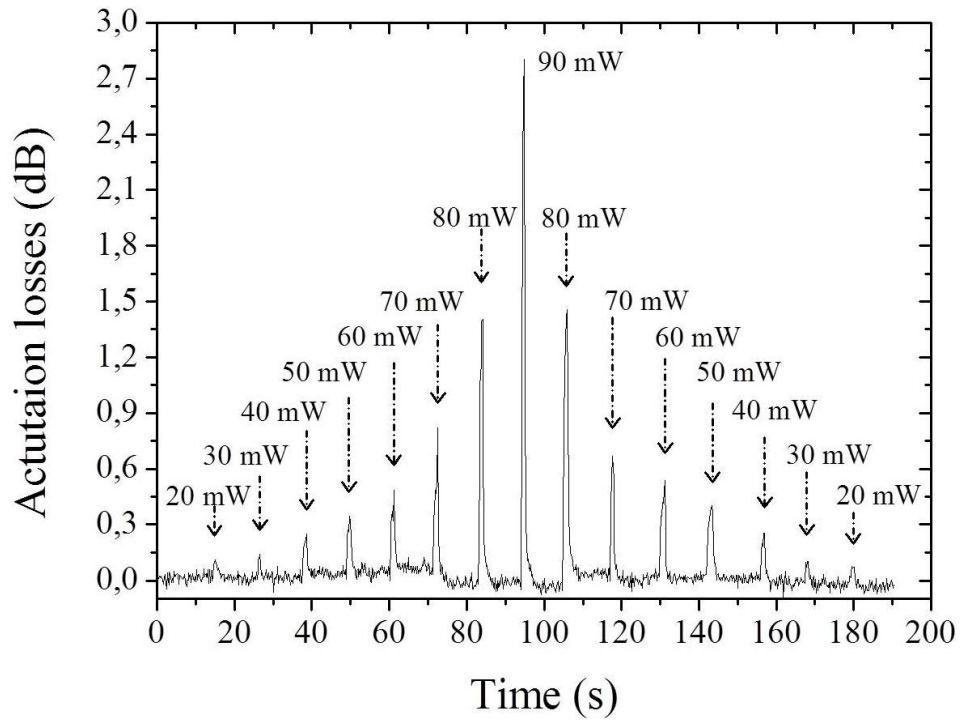


Figure 2.22: Scheme of the setup for the VOA-MOEMS characterization: green laser, input/output fiber and VOA-MOEMS. Moreover, the detail of the right image shows the waveguide-cantilever as well as the actuation point where the green laser is focused.

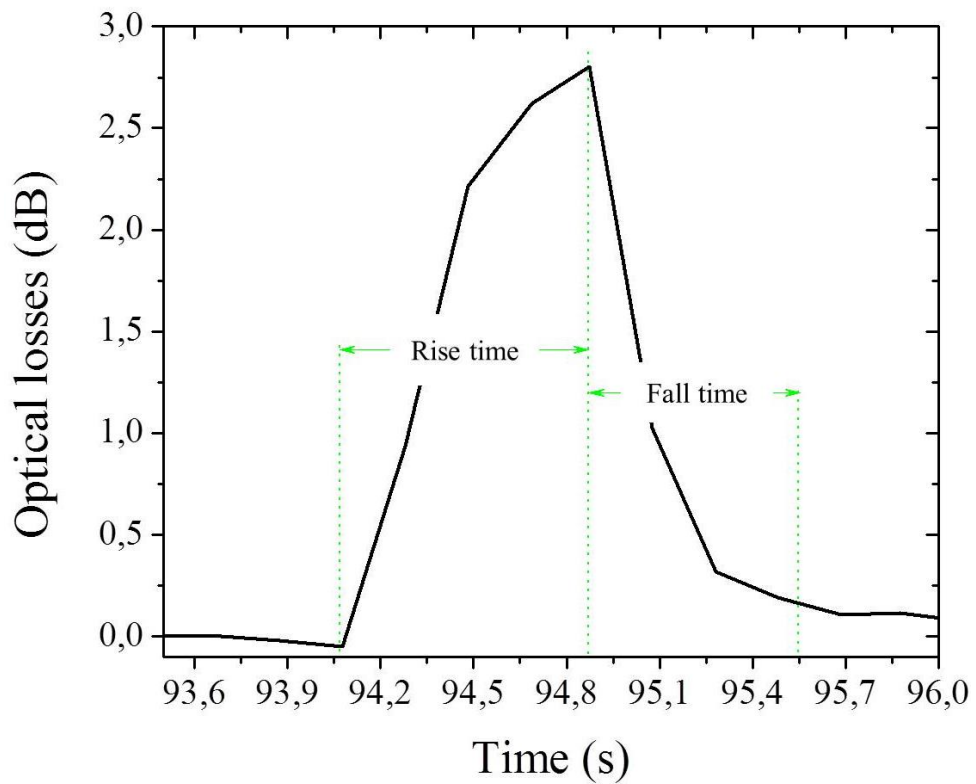
The intrinsic losses were firstly measured with the actuation laser turned off. This magnitude provides information regarding the guiding quality of the waveguide. Thus, when there is no opto-thermal actuation, the optical losses are 0.01 dB which corresponds to a transmittance of the waveguide close to 99.5 %, which is in agreement with the data sheet of the SU-8 [21].

The actuation laser turned on causes an expansion of the color dye-doped SU-8and, straightforwardly, entails a displacement of the seismic mass. As it can be observed in Figure 2.23(a) the experimental results in a full cycle (from 0 mW to 90 mW to 0 mW) show excellent reversibility and repeatability as a function of the actuation power, reaching values close to 3dB for 90 mW. Moreover, the intrinsic losses indicate the guiding quality of the waveguide. Thus, when there is no opto-thermal actuation, the optical losses are 0.01 dB which corresponds to a transmittance of the waveguide close to 99.5 %, which is in In Figure 2.23(b) the time evolution for the case corresponding to 90 mW can be observed. Thus one can conclude that the response time, i.e. the rise time (1.7 s) and fall time (3.5 s), is 5.2 s.

2. Results & Discussion



(a)



(b)

Figure 2.23: (a) Actuation losses for VOA-MOEMS based on L-SSM_{SU-8} as a function of the time when the pumping light power (at $\lambda=532$ nm) was focused at the actuation point and b) expanded base corresponding to the peak of 90 mW, where both the rise and the fall time are marked with green arrows.

REFERENCES

- [1] G. Filipcsei and M. Zrínyi, “Magnetodeformation effects and the swelling of ferrogels in a uniform magnetic field,” *J. Phys. Condens. Matter*, vol. 22, no. 27, p. 276001, Jul. 2010.
- [2] F. Pirmoradi, L. Cheng, and M. Chiao, “A magnetic poly(dimethylsiloxane) composite membrane incorporated with uniformly dispersed, coated iron oxide nanoparticles,” *J. Micromechanics Microengineering*, vol. 20, no. 1, p. 015032, Jan. 2010.
- [3] M. Balasoiu, V. T. Lebedev, D. N. Orlova, and I. Bica, “Magnetic field and particle concentration competitive effects on ferrofluid based silicone elastomer microstructure,” *Crystallogr. Reports*, vol. 56, no. 7, pp. 1177–1180, Nov. 2011.
- [4] M. Balasoiu, V. T. Lebedev, D. N. Orlova, I. Bica, and Y. L. Raikher, “SANS investigation of a ferrofluid based silicone elastomer microstructure,” *J. Phys. Conf. Ser.*, vol. 351, no. 1, p. 012014, Mar. 2012.
- [5] Q. A. Pankhurst, J. Connolly, S. K. Jones, and J. Dobson, “Applications of magnetic nanoparticles in biomedicine,” *J. Phys. D. Appl. Phys.*, vol. 36, no. 13, pp. R167–R181, Jul. 2003.
- [6] D. . Kim, Y. Zhang, W. Voit, K. . Rao, J. Kehr, B. Bjelke, and M. Muhammed, “Superparamagnetic iron oxide nanoparticles for bio-medical applications,” *Scr. Mater.*, vol. 44, no. 8–9, pp. 1713–1717, May 2001.
- [7] G. F. Goya, T. S. Berquó, F. C. Fonseca, and M. P. Morales, “Static and dynamic magnetic properties of spherical magnetite nanoparticles,” *J. Appl. Phys.*, vol. 94, no. 5, p. 3520, Sep. 2003.
- [8] R. Kaiser, “Magnetic Properties of Stable Dispersions of Subdomain Magnetite Particles,” *J. Appl. Phys.*, vol. 41, no. 3, p. 1064, Mar. 1970.
- [9] J. C. McDonald, D. C. Duffy, J. R. Anderson, D. T. Chiu, H. Wu, O. J. A. Schueller, and G. M. Whitesides, “Fabrication of microfluidic systems in poly(dimethylsiloxane),” *Electrophoresis*, vol. 21, no. 1, pp. 27–40, 2000.
- [10] T. Mosmann, “Rapid colorimetric assay for cellular growth and survival: Application to proliferation and cytotoxicity assays,” *J. Immunol. Methods*, vol. 65, no. 1–2, pp. 55–63, Dec. 1983.
- [11] P. P. Castañeda, “A New Variational Principle and Its Application to Nonlinear Heterogeneous Systems,” Jul. 2006.
- [12] J. Rault, J. Marchal, P. Judeinstein, and P. A. Albouy, “Stress-Induced Crystallization and Reinforcement in Filled Natural Rubbers: ^2H NMR Study,” *Macromolecules*, vol. 39, no. 24, pp. 8356–8368, Nov. 2006.

2. Results & Discussion

- [13] Y. Merckel, J. Diani, M. Brieu, and J. Caillard, "Effects of the amount of fillers and of the crosslink density on the mechanical behavior of carbon-black filled styrene butadiene rubbers," *J. Appl. Polym. Sci.*, vol. 129, no. 4, pp. 2086–2091, Aug. 2013.
- [14] A. Llobera, R. Wilke, and S. Büttgenbach, "Enhancement of the response of poly(dimethylsiloxane) hollow prisms through air mirrors for absorbance-based sensing," *Talanta*, vol. 75, no. 2, pp. 473–9, Apr. 2008.
- [15] Y. Xia and G. M. Whitesides, "Soft Lithography," *Angew. Chemie Int. Ed.*, vol. 37, no. 5, pp. 550–575, Mar. 1998.
- [16] M. J. Madou, *Manufacturing Techniques for Microfabrication and Nanotechnology*. CRC Press, 2011.
- [17] F. N. Pirmoradi, J. K. Jackson, H. M. Burt, and M. Chiao, "A magnetically controlled MEMS device for drug delivery: design, fabrication, and testing," *Lab Chip*, vol. 11, no. 18, pp. 3072–80, Sep. 2011.
- [18] S. Bosch, J. Ferré-Borrull, N. Leinfellner, and A. Canillas, "Effective dielectric function of mixtures of three or more materials: a numerical procedure for computations," *Surf. Sci.*, vol. 453, no. 1, pp. 9–17, 2000.
- [19] D. A. Chang-Yen, R. K. Eich, and B. K. Gale, "A monolithic PDMS waveguide system fabricated using soft-lithography techniques," *J. Light. Technol.*, vol. 23, no. 6, pp. 2088–2093, Jun. 2005.
- [20] A. Llobera, R. Wilke, and S. Büttgenbach, "Poly(dimethylsiloxane) hollow Abbe prism with microlenses for detection based on absorption and refractive index shift," *Lab Chip*, vol. 4, no. 1, pp. 24–7, Feb. 2004.
- [21] "<http://www.microchem.com>."
- [22] E. Carregal-Romero, C. Fernández-Sánchez, A. Eguizabal, S. Demming, S. Büttgenbach, and A. Llobera, "Development and integration of xerogel polymeric absorbance micro-filters into lab-on-chip systems," *Opt. Express*, vol. 20, no. 21, pp. 23700–19, Oct. 2012.
- [23] A. Llobera, S. Demming, H. N. Joensson, J. Vila-Planas, H. Andersson-Svahn, and S. Büttgenbach, "Monolithic PDMS passband filters for fluorescence detection," *Lab Chip*, vol. 10, no. 15, pp. 1987–92, Aug. 2010.
- [24] M. Yamazaki, O. Hofmann, G. Ryu, L. Xiaoe, T. K. Lee, A. J. deMello, and J. C. deMello, "Non-emissive colour filters for fluorescence detection," *Lab Chip*, vol. 11, no. 7, pp. 1228–33, Apr. 2011.
- [25] T. Guan, F. Ceysens, and R. Puers, "An EpoClad/EpoCore-based platform for MOEMS fabrication," *J. Micromechanics Microengineering*, vol. 23, no. 12, p. 125005, Dec. 2013.

2. Results & Discussion

- [26] S. de Pedro, A. Voigt, V. J. Cadarso, J. Vila-Planas, J. Brugger, S. Büttgenbach, A. Llobera, and G. Gruetzner, “UV-patternable polymers with selective spectral response,” *Microelectron. Eng.*, vol. 98, pp. 234–237, Oct. 2012.